

A revised catalogue of EGRET γ -ray sources

Jean-Marc Casandjian¹ and Isabelle A. Grenier¹

Laboratoire AIM, CEA/DSM - CNRS - Université Paris Diderot,
Service d'Astrophysique, CEA Saclay, 91191 Gif sur Yvette, France
e-mail: casandjian@cea.fr & isabelle.grenier@cea.fr

Received ; accepted

ABSTRACT

Aims. We present a catalog of point γ -ray sources detected by the EGRET detector aboard the Compton Gamma Ray Observatory. We have used the whole γ -ray dataset of reprocessed photons at energies above 100 MeV together with new Galactic interstellar emission models based on recent CO, HI, dark gas, and interstellar radiation field data. Two different assumptions have been used for the cosmic-ray distribution in the Galaxy to explore the resulting systematic uncertainties in source detection and characterization.

Methods. We have used the same 2-dimensional maximum-likelihood detection method as for the 3rd EGRET catalogue.

Results. The revised catalogue lists 188 sources, 14 of which are marked as confused, compared to the 271 entries of the 3rd EGRET (3EG) catalogue. 107 former sources have not been confirmed because of the additional structure in the interstellar background. The vast majority of them were unidentified and marked as possibly extended or confused in the 3EG catalogue. In particular, we do not confirm most of the 3EG sources associated with the local clouds of the Gould Belt. Alternatively, we find 30 new sources with no 3EG counterpart. The new error circles for the confirmed 3EG sources largely overlap the previous ones, but several counterparts of particular interest that had been discussed in the litterature, such as Sgr A*, radiogalaxies and several microquasars are now found outside the error circles. We have cross-correlated the source positions with a large number of radio pulsars, pulsar wind nebulae, supernova remnants, OB associations, blazars and flat radiosources and we find a surprising large number of sources (87) at all latitudes with no counterpart among the potential γ -ray emitters.

Key words. Egret, gamma-ray source, catalog

1. Introduction

The Energetic Gamma-Ray Experiment Telescope (EGRET), which operated on board the Compton-Gamma Ray Observatory from April 1991 to May 2000, detected photons in the 20 MeV to 30 GeV range. The observation program made use of the large instrumental field of view (25° in radius) to cover the whole sky and for in-depth studies of specific regions. The resulting exposure and flux sensitivity to point sources are therefore not uniform across the sky. The sensitivity threshold also varies because of the intense background emission that arises from cosmic-ray interactions with the interstellar gas and photon fields in the Milky Way. The minimum flux that EGRET could detect steeply rises with decreasing Galactic latitude. In order to detect point sources and assess their significance in these varying conditions, a 2-dimensional maximum-likelihood method using binned maps had been developed for the COS-B data (Pollock et al., 1981) and implemented for the EGRET one (Mattox et al., 1996). A first catalog using this method was published after 1.5 years of data (Fichtel et al., 1994), followed by the second one (Thompson et al., 1995) and its supplement (Thompson et al., 1996) after 3 years of data. Lamb & Macomb (1997) presented a catalog of sources detected above 1 GeV. The last EGRET catalog (hereafter 3EG, Hartman et al., 1999) comprised reprocessed data from April 1991 to October 1995 with the interstellar emission model from Hunter et al. (1997) and extragalactic background from Sreekumar et al. (1998). This version contained 271 point sources including a solar flare, the Large Magellanic Cloud, five pulsars, one radiogalaxy de-

tction (Cen A), 66 high-confidence identifications of blazars (BL Lac objects and flat-spectrum radio quasars), and 27 lower-confidence blazar identifications. Because of the wide tails of the instrument point-spread function, seven potential artifacts were noted around the brightest sources and many sources were marked as confused or possibly extended.

The 3EG catalogue also contained 170 sources with no attractive counterpart at lower energy. About 130 of them remain unidentified as of today (see Grenier (2004) and references therein). Candidate counterparts that have been searched for include pulsars and their wind nebulae, supernova remnants, massive stars, X-ray binaries and microquasars, blazars and nearby radiogalaxies, luminous infrared and starburst galaxies, and galaxy clusters. It was also noticed (Grenier, 1995, Grenier, 2000, Gehrels et al., 2000) that the most stable unidentified sources are significantly correlated with the nearby Gould Belt, a system of massive stars and interstellar clouds that surrounds the Sun at a distance of hundreds of parsecs. The offset position of the Sun with respect to the Belt centre and the Belt inclination of 17° to the Galactic plane indeed provides a useful spatial signature across the sky (Perrot & Grenier, 2003).

EGRET went on observing for another 4.5 years after the 4 cycles used for the 3EG work. Its sensitivity was reduced because of the ageing gas in the spark chamber, but it gathered nearly ten percent more photons and saw several new variable sources. Several authors (Nolan et al., 2003, Sowards-Emmerd et al., 2005), however, noticed discrepancies between their studies and at least five 3EG sources. They failed to confirm sources and found others. The whole γ -ray dataset and final instrument response functions have

also been significantly reprocessed by the EGRET team in 2001. Furthermore, the spatial coverage of the CO surveys has reached higher latitudes since 1999, finding new small CO clouds (Dame et al., 2001). In parallel, new HI surveys (Kalberla et al., 2005) have been completed to correct for the significant contamination of stray radiation in the older ones. Finally, an additional 'dark' gas component has been found in the Gould Belt clouds that significantly increases their mass and spatial extent (Grenier et al., 2005). The additional mass is structured into large envelopes around the dense CO cores. They do not follow the HI and CO maps commonly used to trace atomic and molecular column-densities. So, the dark gas provides both γ -ray intensity and structure that were not accounted for in the 3EG background model.

For all these reasons and in preparation of the new GLAST mission, it was necessary to revise the interstellar background model and to apply the EGRET detection method to the full nine years of data to build a new catalogue of sources above 100 MeV. In order to study the systematic uncertainties induced on source locations and fluxes by our limited knowledge of the intense interstellar background, we have applied the analysis to two different background models exploiting the same new interstellar data, but using different approaches to constrain the cosmic-ray gradient across the Galaxy.

2. The Galactic interstellar emission models

The high-energy Galactic emission is produced by the interaction of energetic cosmic-ray electrons and protons with interstellar nucleons and photons. The decay of neutral pions produced in hadron collisions accounts for most of the emission above 300 MeV. Inverse Compton (IC) scattering of the interstellar radiation field by electrons and their Bremsstrahlung emission in the interstellar gas are the other main contributors to the Galactic emission. The observed intensity therefore scales with the integral along the line of sight of the cosmic-ray density times the gas or soft-photon one.

The diffuse model used for the 3EG catalogue (Hunter et al., 1997) was based on a 3D-distribution of matter, cosmic-ray and soft-photon densities in the Galaxy, where the cosmic-ray density was assumed to be coupled to the gas one over a given length scale. This length as well as the CO -to- H_2 conversion factor (X ratio) were adjusted to the data. The 3D gas map was obtained from the HI and CO line surveys and from kinematical distances derived for circular rotation. Distance ambiguities in the inner Galaxy were solved by splitting the gas into the far and near sides according to its expected scale height. Gas with velocities in excess of the tangent values was attributed to the tangent point and gas emission within 10° of the Galactic center and anticenter was interpolated from the regions just outside these boundaries and normalized to match the total emission seen along the line of sight. The resulting map is, however, still strongly biased to our side of the Galaxy, particularly for the atomic gas. This bias is reflected in the cosmic-ray density via the coupling length.

For the present analyses, we have assumed an axisymmetric Galaxy for the cosmic-ray density and we have used gas column-density distributions in Galactocentric rings that are less subject to biases due to the strategy adopted to solve the cloud distance in the inner Galaxy. The radial velocity information in the HI and CO line surveys, together with the rotation curve of Clemens (1985) and the solar motion ($v = 220$ km/s at $R = 8.5$ kpc), have been used to partition the gas into 6 rings bounded by 3.5, 7.5, 9.5, 11.5, and 13.5 kpc in Galactocentric distance (Digel et al., in

preparation). Gas within 10° of the Galactic center and anticenter was interpolated as before. The all-sky Leiden-Argentina-Bonn (LAB) composite survey (Kalberla et al., 2005) was used for the HI data. Column densities, $N(HI)$, were derived under the assumption of a constant spin temperature of 125 K. The velocity-integrated CO brightness temperature, $W(CO)$, comes from the Center for Astrophysics compilation of observations at $|b| \leq 32^\circ$ (Dame et al., 2001). The regions outside the survey boundaries should be free of bright CO emission.

We have used two different approaches to account for the cosmic-ray density gradient. One is based on the Galprop model for cosmic-ray propagation developed by Strong et al. (2007, 2004a, 2004b), using run number 49-6002029RB to derive the γ -ray maps from pion decay, I_{π^0} , bremsstrahlung radiation, I_{brem} , and inverse Compton radiation, I_{IC} . This version includes secondary electrons and positrons, an optimized cosmic-ray spectrum to fit the GeV excess in the EGRET data, a cosmic-ray source distribution matching the radial profile of pulsars and supernova remnants, a radial gradient in the X factor, and the new HI and CO gas rings.

The second model, hereby referred to as the Ring model, is based on the simpler, but realistic hypothesis that, if energetic cosmic rays uniformly penetrate all gas phases, the γ -ray intensity in each direction can be modelled as a linear combination of gas column-densities in the different rings, plus the IC intensity map (as predicted by Galprop), and an isotropic intensity (I_{iso}) that accounts for very local IC emission and extragalactic emission. This assumption has been used to derive gas emissivities in several rings from the COS-B and EGRET data (Strong et al., 1988, Strong & Mattox, 1996). We have reproduced these analyzes to derive gas emissivities for the new HI and CO rings using 9 years of EGRET data in three energy bands (> 100 MeV, $0.3 - 1$ GeV, > 1 GeV). Both the Ring and Galprop models used the revised distribution of the interstellar radiation field (Porter & et al., 2005, Moskalenko et al., 2006) to calculate the IC intensity map. The Galprop IC map is common to both diffuse models.

As indicated in the introduction, we have also included in the local ring the large column-densities of "dark" gas associated with cold and anomalous dust at the transition between the atomic and molecular phases (Grenier et al., 2005). This transitional phase is not traced in the radio. When removing from total dust column-density maps the part that linearly correlates with $N(HI)$ and $W(CO)$, one is left with large envelopes of excess dust around all the nearby CO clouds. The fact that the excess dust spatially correlates with significant diffuse gamma radiation indicates that cosmic rays pervade gas not accounted for in HI or CO . The gas-to-dust ratio in this phase, as inferred from the excess dust and correlated γ -ray data, is normal. This phase appears to form an extended layer at the transition between the dense CO cores and the densest parts of the outer HI envelope of a cloud complex. It is best seen in total dust maps such as the reddening E(B-V) map (Schlegel et al., 1998), or low-frequency thermal emission at 93 GHz for WMAP (Finkbeiner et al., 1999), or anomalous emission near 20 GHz (Lagache, 2003). We constructed a "dark" gas column-density template, NH_{dark} , by removing from the E(B-V) map the part linearly correlated with $N(HI)$ and $W(CO)$. This template was turned into gas column-densities by fitting it together with the $N(HI)$ and $W(CO)$ rings, as well as IC and isotropic components, to the all-sky γ -ray maps. Because of its column-densities, clumpiness, and large spread across the sky (see Figure 4 in Grenier et al. (2005)), the "dark" gas component

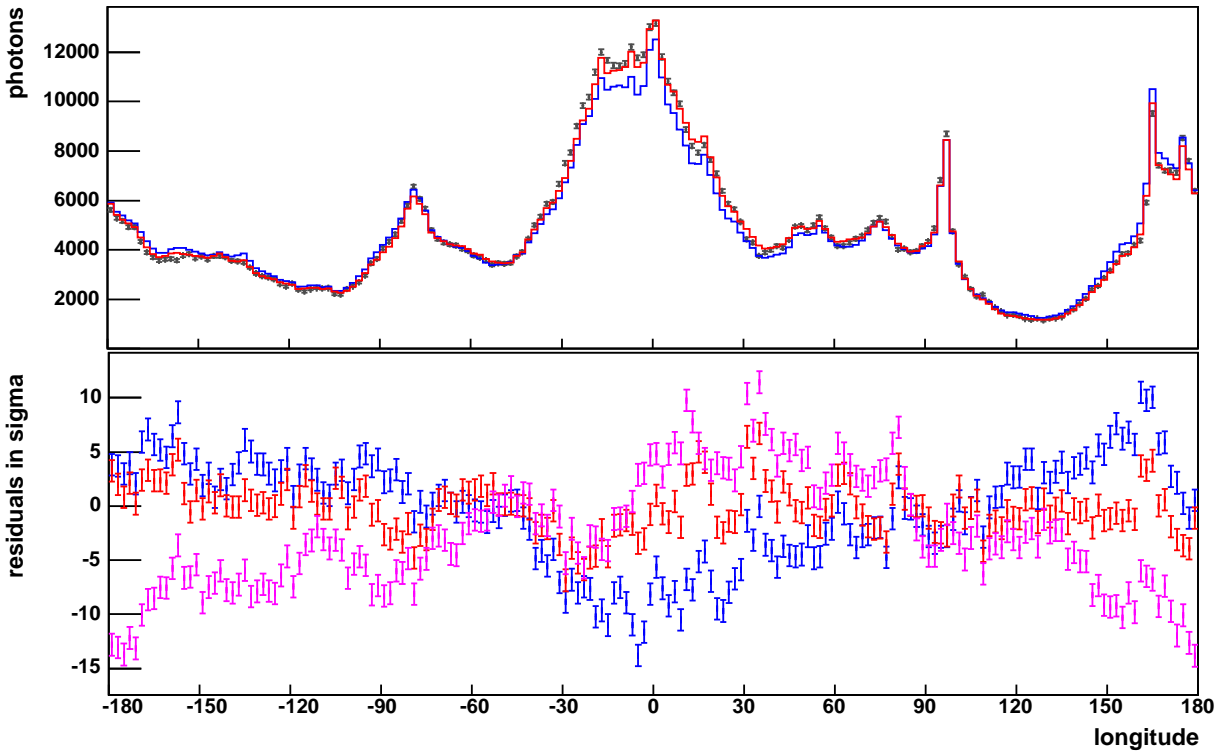


Fig. 1. The top figure is the longitude profile of all photon counts observed by EGRET above 100 MeV at all latitudes (black error bars), compared with the diffuse counts predicted by the 3EG model (blue curve) and the Ring model (red curve). The bottom figure is the residual expressed in number of standard deviation, colors are the same as above, we added the Galprop residuals in purple. Counts from bright sources have been added to the diffuse component. For more visibility the plot are presented with a binning of 4° .

may strongly affect source detectability. This template was also added to the Galprop 49-6002029RB background model.

To summarize, two diffuse backgrounds were constructed by fitting different components to the EGRET photon maps, in $0.5^\circ \times 0.5^\circ$ bins, in the three energy bands that will be used for source detection (> 100 MeV, $0.3 - 1$ GeV, > 1 GeV).

- With the Ring model, the predicted count rates are calculated as:

$$N_{pred}(l, b) = [\sum_{i=rings} q_{HI,i} N_{HI}(r_i, l, b) + \sum_{rings} q_{CO,i} W_{CO}(r_i, l, b) + q_{dark} N H_{dark}(l, b) + q_{IC} I_{IC}(l, b) + I_{iso}] \times \epsilon(l, b) + \sum_{j=sources} \epsilon(l_j, b_j) f_j PSF(l_j, b_j)$$

- and the Galprop model as:

$$N_{pred}(l, b) = [q_{\pi^0} I_{\pi^0}(l, b) + q_{brem} I_{brem}(l, b) + q_{dark} N H_{dark}(l, b) + q_{IC} I_{IC}(l, b) + I_{iso}] \times \epsilon(l, b) + \sum_{j=sources} \epsilon(l_j, b_j) f_j PSF(l_j, b_j)$$

In both models, $\epsilon(l, b)$ and f_j note the EGRET exposure map and source fluxes. The diffuse maps times the exposure were convolved with the EGRET PSF for an input $E^{-2.1}$ spectrum before adding the source maps. The EGRET count and exposure maps, the 3EG diffuse model, as well as the latest instrument response functions, were downloaded from the CGRO Science Support Center. They differ from those used for 3EG since they were reprocessed in 2001. The q parameters (gas emissivities or relative contributions of different radiation components)

were fitted to the data by means of a maximum likelihood with Poisson statistics. To avoid biasing the interstellar parameters, the model included the brightest sources detected during a first source detection iteration with a significance $> 5\sigma$, with fixed fluxes. Changing these fluxes within their statistical uncertainties do not significantly change the diffuse results.

The resulting emissivities corresponding to the local gas are fully consistent with Grenier et al. (2005) Table 1. The emissivity gradient in the Galactic plane will be described in a separate paper. The quality of the fit can be seen in Figure 1. The top figure displays the longitude profile of all the EGRET photon counts above 100 MeV. The error bars are only statistical. The plot compares the best fit that can be obtained using the former 3EG diffuse model with the longitude profile resulting from the present Ring model. The bottom plot shows the longitude profile of the residuals and the improvement of the ring model over the 3EG one. It also shows the residuals for the best fit Galprop model. All modelled profiles include the brightest sources. Systematic differences can be seen in various places where the 3EG model significantly over-predicts and under-predicts the data while the new models behave better. Because of its larger flexibility (the gas emissivity gradient due to cosmic-ray variations is measured, not inferred from propagation properties or gas coupling), the Ring model was found to best fit the data. It is worth noting that even if the agreement is excellent, there still exists small devia-

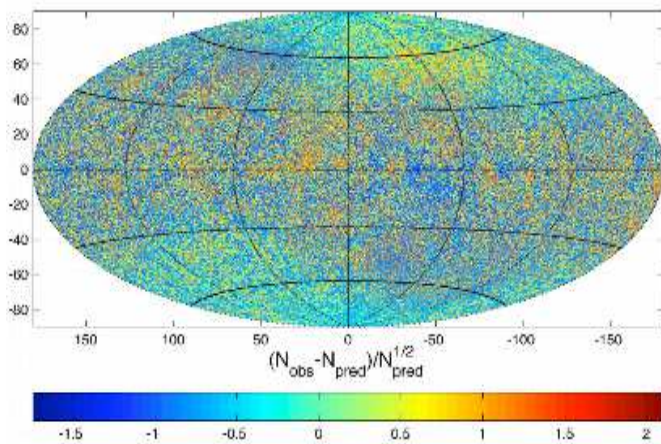


Fig. 2. Map in Galactic coordinates of the residuals (expressed in $\sigma = \sqrt{N_{\text{pred}}}$ values) between the $E > 100$ MeV photon counts (in 0.5° bin) and the best fit with the Ring model using Equation (1)

tions that can significantly impact source detection and characterization.

The residual count map obtained above 100 MeV with the Ring model is presented in Figure 2. It displays the statistical difference $(N_{\text{obs}} - N_{\text{pred}})/\sqrt{N_{\text{pred}}}$ between the observed counts and those predicted from the diffuse background and bright sources using equation 1. The model globally fits very well the data. The extended blue fan-like structures with negative residuals are correlated with the edge of several observing periods. They probably result from a wrong exposure estimate at large angle from the instrument axis. They are visible independently of the choice of diffuse model (Ring, Galprop, or 3EG). Their spatial extent is large enough compared to the PSF size not to severely affect source detection, yet source fluxes in these directions are underestimated. Uncertain knowledge of the off-axis instrument exposure is also reflected in the small model deficit (orange edge) bordering the fan-like excesses. We have checked for suspicious strings of faint sources that would correlate with these instrumental features.

The use of two different background models allowed us to study their impact on source detection and characterization. Given its higher likelihood value and locally flatter residuals, the Ring model was used to derive the default source flux and location. The values obtained with the Galprop background are used to illustrate the amplitude of the systematic uncertainty due to the background modelling. When searching for sources we used the diffuse emission parameters calculated from this global fit. We adjusted a source flux together with a free normalization of the total diffuse flux within 15° around each pixel, and a free isotropic flux. This procedure is the same as used for 3EG (Gmult and Gbias). These two parameters correct for small local mismatches between the diffuse model and the data. Gmult fluctuates around 1.

3. Source detection

As for the derivation of the 3EG catalogue, we have used the LIKE code (Mattox, 1996, version 5.61) to compute the 2-dimension binned Poisson likelihood of detecting a source at a particular location on top of the diffuse background. LIKE cal-

culates the Test Statistic (TS) value that compares the likelihood of detecting a PSF-like excess above the background to the null hypothesis - a random background fluctuation - for a given position. The likelihood (L_i) is calculated as the product, for all pixels within 15° of a specific position, of the Poisson probabilities of observing photons in a pixel where the number of counts is predicted by the model (background + source). The likelihood ratio test statistic is defined as $TS = -2(L_1 - L_0)$, where the likelihood values L_1 and L_0 are respectively optimized with and without a source in the model. Asymptotically, the TS distribution follows a χ^2 one. The detection significance of a source at the given position is $\sqrt{TS}\sigma$ (Mattox 1996).

Sources have been searched for in the summed maps corresponding to cycle 1, 2, 3, 4, 1+2, 3+4, 1+2+3+4, 5+6, 7+8+9, 1+2+3+4+5+6+7+8+9. In addition, we have analyzed the 46 individual periods listed in Table 1 for which flaring 3EG sources had been detected. As for the summed maps, the individual period maps retained only photons with inclinations within 30° from the instrument axis, or 19° for cycle 6, 7, 8, and 9. Photons and exposure maps were binned to $0.5^\circ \times 0.5^\circ$.

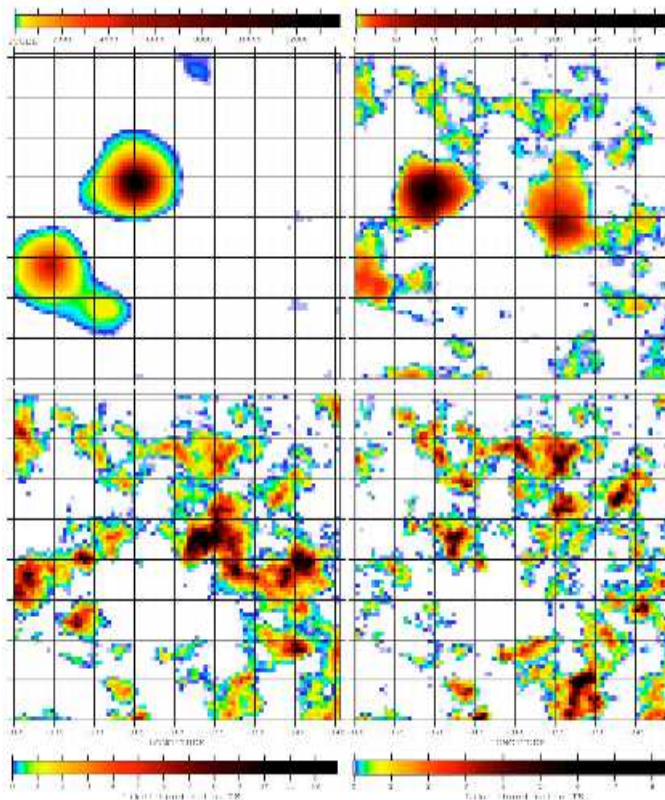
To build the 3EG catalogue, sources were detected only in the integrated $E > 100$ MeV band. TS maps were then constructed in three energy bands (> 100 MeV, $0.3 - 1$ GeV, and > 1 GeV) from the observation (single or summed) with highest TS and a source final position was obtained from the smallest error contours. Given the modern computer performance, we have directly searched for sources independently in the three energy bands.

At 100 MeV, the EGRET PSF is wide and there exists discrepancies between its real shape, as observed in bright sources, and the modelled one. In practice, differences may also come from a more complex source spectrum than the single power-law assumed to integrate the PSF. A choice of 300 MeV instead of 100 MeV for the lower analysis threshold might have been a better trade-off between count rates for detection and systematic uncertainties in the PSF. We have, however, kept a lower limit of 100 MeV as in 3EG in order to account for soft sources and to allow comparison with the 3EG results. We have assumed a spectral index of 2.0 for all sources but for 11 bright ones which had a 3EG spectral index far from 2.0. For the latter, we have used their 3EG index to integrate the PSF.

Each of the 10 all-sky summed maps was divided, both in Galactic and equatorial coordinates, in 45 zones with a large overlap. The use of both coordinate systems is required since source images are deformed in rectangular projection at high latitude or declination. For each zone, each individual period, and each of the 3 energy bands (> 100 MeV, $0.3 - 1$ GeV, and > 1 GeV), we calculated a TS map for excesses above the background. Sources were iteratively detected from high TS to low TS in successive TS maps. Between each steps, the detected sources were included in the background model until no excess with $\sqrt{TS} > 3$ was left in the final TS map. An example of the iteration around Geminga is given in Figure 3. Peaks in the TS map were automatically detected with SExtractor (Bertin & Arnouts, 1996) and converted into source position by taking the TS -weighted centroid in the region enclosed by the 95% confidence contour around this position. Source positions were recalculated at each iteration to take into account the influence of the neighbouring sources. More than 1100 TS -maps were thus calculated at the CCIN2P3 Computing Center.

Table 1. List of individual or short periods used in the analysis in addition to the summed cycles.

Name	Sum of viewing periods	Name	Sum of viewing periods	Name	Sum of viewing periods
2+	0002+0003+0004+0005	2040	2040+2050+2060	3315	
0020		virg2		330+	3300+3320
0040		2110		335+	3350+3355
0050		2230		vrg3a	3040+3050+3060+3070+3080+3086
0200		2260		3355	
0210		227+	2270+2280	3360	
0220		229+	2290+2295	3385	
0230		2310		3390	
0250		3023		4040	
0260		314+	3140+3150	4100	
0290		3170		4130	
36+	0360+0365	319+	3190+3195	4180	
0420		3200		419+	4191+4195
0430		328+	3280+3310+3315+3330	4210	
0440		3290		4230	
				4235	

**Fig. 3.** An example of the iterative source detection with the 2D binned likelihood around Geminga at energies above 100 MeV. 4 consecutive TS maps are shown. Sources are detected, then are included in the background for the next step until no significant one is left. The colourbar gives TS .

4. Catalogue construction

To account for real versus modelled PSF discrepancies in extremely bright sources, for instance to account for the splitting in two of the bright pulsar sources or for the artifacts in the Vela tails, we have removed all the source candidates within 3.5° of the intense sources (that exhibit more than 800 photons in a map). For less intense sources, we have checked the probability of having a double versus single source with a specific likelihood calculation, using the likelihood ratio between the 2 cases to keep or reject the double source.

At the end of this stage, most sources have two possible positions per energy band and observation, one from the Galactic coordinate map and one from the equatorial one. We cross-compared the two and selected the position from the least deformed projection. Sources detected only once were not included in the list unless their latitude or declination were higher than 40° or their longitude or right-ascension were less than 5° from the map edges.

At this stage, most sources have three possible positions (with energy) for a given observation. We chose among the three the position corresponding to the smallest 95% confidence contour, unless its peak \sqrt{TS} were 1.5 smaller than found in another energy band. The latter condition reduces the risk of incorrect source assignment during the cross-comparison phase. Sources found at low energy, but not at high energy were included in the list, as well as sources found only at high energy.

We have used the same criteria to cross-compare the source positions for individual periods and summed cycles in order to obtain a final list of candidate sources with the best position from the different energy bands and periods/cycles. We followed the whole procedure with both the Ring and Galprop interstellar backgrounds. We obtained respectively 1192 and 1225 candidate sources with the Ring and Galprop models. Source fluxes and \sqrt{TS} values above 100 MeV were calculated for these sets of positions for the different periods and cycles. Unlike in 3EG, we did not adjust the position of the identified sources (AGN or pulsars) to that of their radio counterpart.

We adopted the same detection threshold as for the 3EG catalogue ($\sqrt{TS} > 5$ at $|b| < 10^\circ$ and $\sqrt{TS} > 4$ elsewhere) and found 188 and 208 significant sources for the Ring and Galprop models, respectively. We manually checked the TS maps of all the sources that barely passed the detection threshold with the Ring model and had $\sqrt{TS} \sim 3$ with the Galprop one.

We emphasize the fact that the order and criteria applied to cross-correlate positions between the excesses detected in different energy bands and time periods can strongly affect the catalog list near the detection threshold. Several strategies were tested before adopting the present one, but one must remember that a faint source can pass or drop below the threshold by slightly changing its position or that of its neighbours. Given the steep increase in source numbers with decreasing TS , we also emphasize that a small change in the TS threshold, alternatively in the

background over which the source TS is calculated, results in a large change in the number of catalogue entries. For instance, lowering the \sqrt{TS} threshold by 0.1 would add 27 sources.

5. Catalogue description

The EGR acronym has been adopted for the EGret Revised source list presented in Table 2 and Table A.1 in a format similar to the 3EG one. As explained above, the source characteristics (position and flux, and their uncertainties) have been determined with the Ring model because of its higher flexibility, better fit, and flatter residual map. A secondary position and flux has been measured with the Galprop model and is listed in Table 2 and Table A.1 to illustrate the amplitude of the systematic uncertainties due to the choice of interstellar model.

Sources found within a radius of 1.5 PSF FWHM from a very bright source, and/or with very asymmetric TS map contours are not included in Table 2 and Table A.1. Still, they represent significant excesses of photons above the background which may be due to extended sources, or structures not properly modelled in the interstellar emission, or artifacts due to incorrect PSF tails. This list of 14 confused sources is given in Table B.1, under the acronym EGRc for EGret Revised confused.

For both tables, the description for each column follows:

1. Num: source number in order of increasing right ascension.
2. Name: source name based on J2000 coordinates.
3. RA and Dec: J2000 equatorial coordinates in degrees.
4. l and b: Galactic coordinates in degrees.
5. θ_{95} : angular radius, in degrees, of a circular cone which contains the same solid angle as the 95% confidence contour.
6. F: flux in 10^{-8} photon $\text{cm}^{-2} \text{s}^{-1}$ for $E > 100$ MeV and for each time period.
7. σ_F : 1σ statistical flux uncertainty in 10^{-8} photon $\text{cm}^{-2} \text{s}^{-1}$.
8. Cnts: number of photons detected with $E > 100$ MeV.
9. \sqrt{TS} : statistical significance of the detection.
10. vp: short viewing period as defined in Table 1 or summed cycles noted px for cycle x, $pijkl$ for the sum of cycles i, j, k, and l, and $p19$ for the total of 9 cycles.
11. l_{sys} and b_{sys} : Galactic longitude and latitude obtained with the Galprop background model.
12. F_{sys} : flux obtained with the Galprop background model, in 10^{-8} photon $\text{cm}^{-2} \text{s}^{-1}$.
13. 3EG: third EGRET catalog counterpart source name if one exists within a radius of 1 PSF FWHM (2° for $E > 100$ MeV) from the EGR source and if the nearest neighbour relation between the EGR and 3EG sources is univocal (the nearest neighbour of the EGR source is the 3EG one and vice versa).

6. Comparison with the 3EG catalogue

The revised catalogue contains 174 sources plus 14 confused sources compared to the 265 entries of the 3EG catalogue (excluding the Vela artifacts). Their spatial distribution across the sky looks different from that of the 3EG sources, as illustrated in Figures 4 and 5. The accumulation of faint 3EG sources within 30° of the Galactic center is much more reduced in the new results and fewer sources are seen below 30° in general. These changes at low and mid latitudes are primarily due to the increase in background intensity from new HI, CO, and dark gas structures. At high latitude, the use of more γ -ray observations and of a revised large-scale IC component in the background may also explain why a handful of 3EG sources have fallen below the detection threshold whereas new ones are now detected.

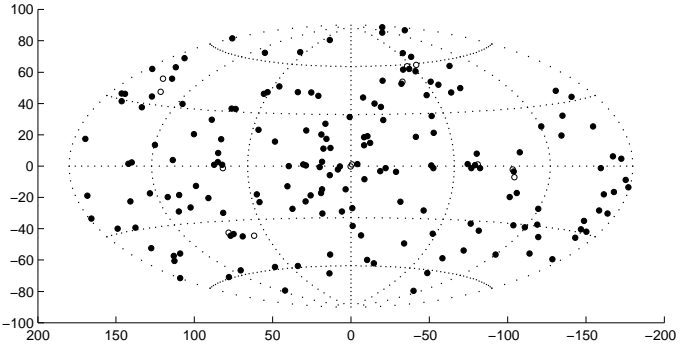


Fig. 4. Spatial distribution, in Galactic coordinates, of the EGR sources. The confused sources are marked as open circles.

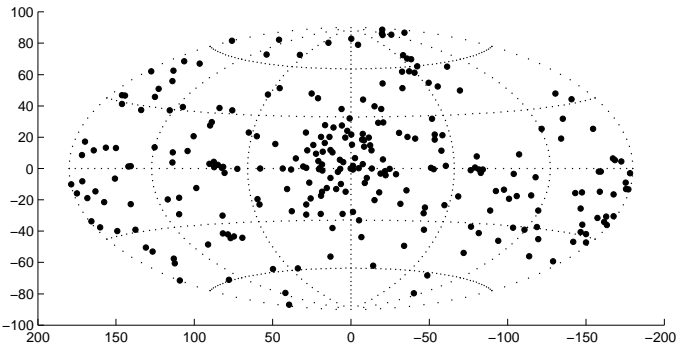


Fig. 5. Spatial distribution, in Galactic coordinates, of the 3EG sources.

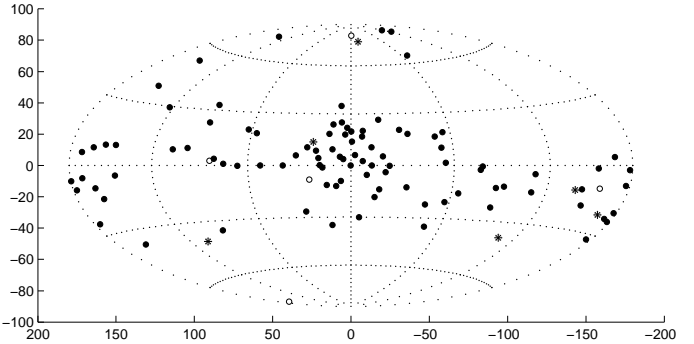
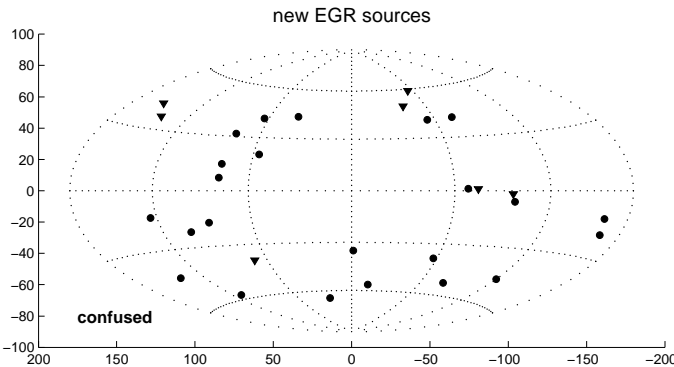


Fig. 6. Spatial distribution, in Galactic coordinates, of the 3EG sources with no counterpart in EGR: the unidentified sources as circles and the identified AGN as stars. The filled circles and stars mark the sources that were flagged as extended or confused in the 3EG catalogue.

The names of the 107 unconfirmed 3EG sources are listed in Table 3 and they are displayed in Figure 6. They comprise only six sources that had been firmly identified as AGN by Hartman et al. (1999), but that had been flagged as extended or confused by the EGRET team. In fact, the proportion of these extended or confused cases among the unconfirmed 3EG sources is overwhelming (95%) and significantly larger than among the confirmed ones. The unconfirmed and confirmed 3EG groups respectively show 69% and 33% of possibly extended 'em' sources. Figure 6 also shows that the vast majority of unconfirmed 3EG sources were unidentified and spatially correlated with the Gould Belt system of nearby clouds. They follow the characteristic trace of the inclined Belt across the sky, gathering at $|b| < 30^\circ$, more at positive latitudes toward the Galactic centre

Table 2. The EGR catalogue. The three first sources are shown. The full catalogue is available with the on-line version

Num 1	Name EGR J0008+7308	RA 2.01	Dec 73.14	l 119.75	b 10.54	θ_{95} 0.20	F 39.7	σ_F 4.4	Cnts 330	\sqrt{TS} 10.9	vp p19	l_{sys} 119.75	b_{sys} 10.54	F_{sys} 41.0	3EG 3EGJ0010+7309
				63.9	11.6		96	7.2			p1				
				33.4	9.6		61	4.1			p2				
				22.4	8.7		37	3.0			p4				
				48.8	7.4		162	8.2			p12				
				21.6	7.3		52	3.4			p34				
				37.0	5.3		212	8.5			p1234				
				44.6	8.3		115	6.6			p56				
				33.1	9.7		60	4.0			2110				
2	EGR J0028+0457	7.06	4.95	112.15	-57.44	0.51	14.3	4.6	31	4.1	p34	112.15	-57.44	14.4	
				7.2	4.8		13	1.7			p1				
				13.9	5.9		20	3.0			p3				
				14.0	7.2		10	2.7			p4				
				7.2	4.8		13	1.7			p12				
				10.7	3.3		43	4.0			p1234				
				10.4	3.1		46	4.1			p19				
				24.2	11.1		14	2.9			3200				
				24.7	15.6		6	2.3			3360				
3	EGR J0039-0945	9.75	-9.75	112.76	-72.38	0.27	13.0	3.5	48	4.8	p19	112.65	-72.40	13.1	3EGJ0038-0949
				14.6	5.8		23	3.4			p1				
				15.7	5.4		24	4.0			p4				
				14.6	5.8		23	3.4			p12				
				11.0	4.5		22	3.2			p34				
				12.3	3.6		43	4.5			p1234				
				22.2	17.7		5	1.6			p789				

**Fig. 7.** Spatial distribution, in Galactic coordinates, of the new EGR sources with no 3EG counterpart. The confused sources are marked as open circles.

and below the plane in the anticenter. The EGR source sky distribution in Figure 4 does not exhibit the Gould Belt signature anymore.

The fact that many 3EG sources are not confirmed in the present analyses should not cast doubts on the detection method from a statistical point of view. They did correspond to significant photon excesses above the background in the 3EG analyses, but, in the absence of some structures in the predicted interstellar background, an ensemble of point sources with the wide EGRET PSF would compensate for the missing clouds and yield an excellent fit to the data. Figure 8 illustrates this point with the unidentified source 3EG J0556+0409 detected at 7.2σ in 3EG. The left side shows the TS-map corresponding to the second stage of the iterative source detection around Geminga above 100 MeV. It is the same as in Figure 3 but we have used here the 3EG diffuse emission model instead of the Ring one. The same sources are detected except for 3EG J0556+0409 which is not seen in Figure 3. Instead an excess of diffuse emission appears in the ratio of the Ring to 3EG background intensities (Figure 8, right). *The photons attributed to a point source in 3EG where in fact coming from a gas cloud in the Galaxy.* This is probably still the case in the present analysis, although to a lesser degree, in particular at very low latitude where optical thickness

Table 3. Names of the 3EG sources with no EGR counterpart

3EG J0130-1758	3EG J0245+1758	3EG J0323+5122
3EG J0348+3510	3EG J0404+0700	3EG J0407+1710
3EG J0416+3650	3EG J0426+1333	3EG J0435+6137
3EG J0439+1555	3EG J0439+1105	3EG J0458-4635
3EG J0459+0544	3EG J0459+3352	3EG J0500+2529
3EG J0510+5545	3EG J0520+2556	3EG J0521+2147
3EG J0533+4751	3EG J0542+2610	3EG J0542-0655
3EG J0546+3948	3EG J0556+0409	3EG J0616-0720
3EG J0622-1139	3EG J0628+1847	3EG J0634+0521
3EG J0702-6212	3EG J0706-3837	3EG J0747-3412
3EG J0808-5344	3EG J0821-5814	3EG J0910+6556
3EG J1013-5915	3EG J1014-5705	3EG J1045-7630
3EG J1052+5718	3EG J1212+2304	3EG J1222+2315
3EG J1227+4302	3EG J1235+0233	3EG J1249-8330
3EG J1300-4406	3EG J1308+8744	3EG J1308-6112
3EG J1316-5244	3EG J1323+2200	3EG J1329+1708
3EG J1329-4602	3EG J1447-3936	3EG J1500-3509
3EG J1527-2358	3EG J1600-0351	3EG J1616-2221
3EG J1627-2419	3EG J1631-1018	3EG J1631-4033
3EG J1633-3216	3EG J1634-1434	3EG J1635-1751
3EG J1639-4702	3EG J1646-0704	3EG J1649-1611
3EG J1653-2133	3EG J1659-6251	3EG J1704-4732
3EG J1709-0828	3EG J1714-3857	3EG J1717-2737
3EG J1718-3313	3EG J1720-7820	3EG J1733+6017
3EG J1735-1500	3EG J1741-2050	3EG J1741-2312
3EG J1744-0310	3EG J1744-3011	3EG J1744-3934
3EG J1757-0711	3EG J1800-0146	3EG J1806-5005
3EG J1810-1032	3EG J1823-1314	3EG J1824+3441
3EG J1824-1514	3EG J1825+2854	3EG J1828+0142
3EG J1834-2803	3EG J1836-4933	3EG J1850+5903
3EG J1850-2652	3EG J1858-2137	3EG J1903+0550
3EG J1904-1124	3EG J1928+1733	3EG J1958+2909
3EG J1958-4443	3EG J2016+3657	3EG J2020-1545
3EG J2022+4317	3EG J2034-3110	3EG J2035+4441
3EG J2100+6012	3EG J2206+6602	3EG J2219-7941
3EG J2255+1943	3EG J2359+2041	

in *HI* and *CO* severely limits our knowledge of the true column-densities. Other sources may also be due to increased cosmic-ray densities in specific clouds with respect to the local Galactic average. Over-irradiated clouds near cosmic-ray sources would be

Table 4. Names of the new EGR sources with no 3EG counterpart

EGR J0028+0457	EGR J0057-7839	EGR J0100+4927
EGR J0141+1719	EGR J0243-5930	EGR J0413-3742
EGR J0509+0550	EGR J0540+0657	EGR J1122-5946
EGR J1158-1950	EGR J1259-2209	EGR J1619+2223
EGR J1642+3940	EGR J1740+4946	EGR J1814+2932
EGR J1920+4625	EGR J1959+4322	EGR J2027-4206
EGR J2202+3340	EGR J2233-4812	EGR J2258-2745
EGR J2308+3645	EGRc J0818-4613	EGRc J0842-4501
EGRc J0912+7146	EGRc J0927+6054	EGRc J1038-5724
EGRc J1255-0404	EGRc J1332-1217	EGRc J2215+0653

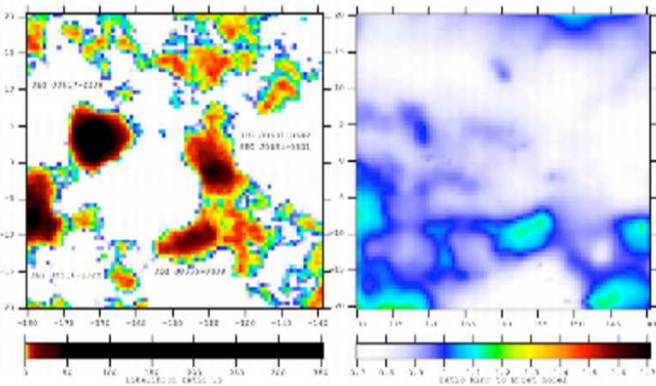


Fig. 8. Second stage of the iterative source detection around Geminga (see Figure 3) obtained using the 3EG model (left) and map of the Ring model intensity divided by the 3EG one (right). The excess in the TS map assigned in 3EG to the 3EG J0556+0409 point source corresponds to a local underestimation of the diffuse emission in the 3EG model. Maps are given in 0.5° bins and galactic coordinates

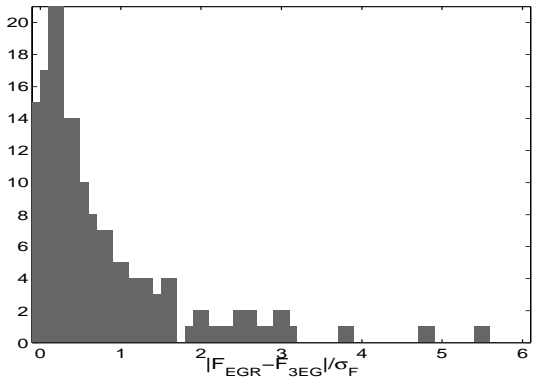


Fig. 9. Histogram of the relative flux differences $|F_{EGR} - F_{3EG}|/\sigma_{F_{EGR}}$ measured between the EGR and 3EG counterparts in units of the statistical error on flux for each source. All fluxes are measured above 100 MeV.

detected as a single or cluster of point sources, depending on their angular scale.

For the 81 EGR sources that do have a 3EG counterpart, we find a reasonable agreement in position and flux from both analyses. On average, we find 3% lower fluxes in the EGR analysis with respect to the 3EG one because of the increase in Galactic background. Figure 9 shows the histogram of ratios of the EGR and 3EG flux difference over the statistical error on flux for each

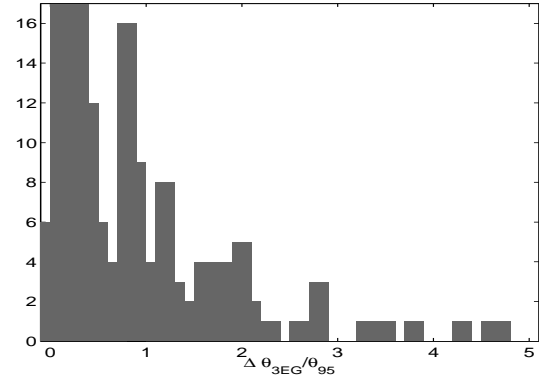


Fig. 10. Histogram of the relative angular separation between the positions found for the EGR and 3EG counterparts in units of the 95% confidence angle for each source.

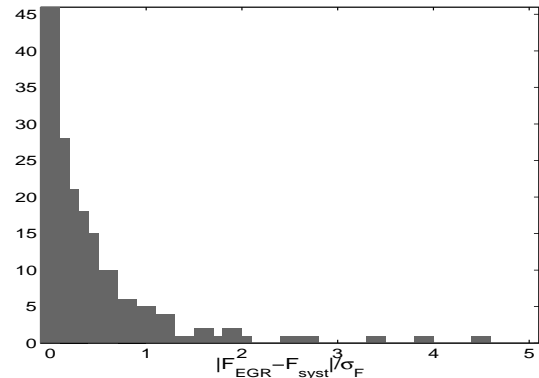


Fig. 11. Histogram of the relative flux differences $|F_{EGR} - F_{3EG}|/\sigma_{F_{EGR}}$ measured with the Ring and Galprop models in units of the statistical error on flux for each source. All fluxes are measured above 100 MeV.

source: $|F_{EGR} - F_{3EG}|/\sigma_{F_{EGR}}$. The EGR flux was taken for the observation with highest \sqrt{TS} and compared to the 3EG counterpart flux for the same time period if available. Average P19 fluxes were compared to the 3EG P1234 average for non flaring sources. The flux differences are modest (17% rms dispersion) and in most cases smaller than the statistical uncertainties on flux estimates. Similarly, Figure 10 shows that the angular separations between EGR and 3EG counterparts are often consistent with the θ_{95} error radii. Yet, thirty sources have been found as far as 0.5° from the 3EG position and this will greatly impact counterpart searches and identification at other wavelengths.

On the other hand, we find 30 new EGR sources with no 3EG counterpart. Their names are listed in Table 4 and they are displayed in Figure 7. Most of them are detected just above the threshold and 11 of them were indeed present in the 3EG complementary list, just below the significance threshold.

7. EGR source distributions and potential counterparts

Because of the new gas data we have used at intermediate latitude, the comparison between the EGR and 3EG source characteristics allows to judge, to some extent, the impact of our limited knowledge of gas mass tracers. The comparison between the flux and positions obtained with the Ring and Galprop models gives an estimate of the systematic uncertainties due to our limited knowledge of the true cosmic-ray distribution across the Galaxy.

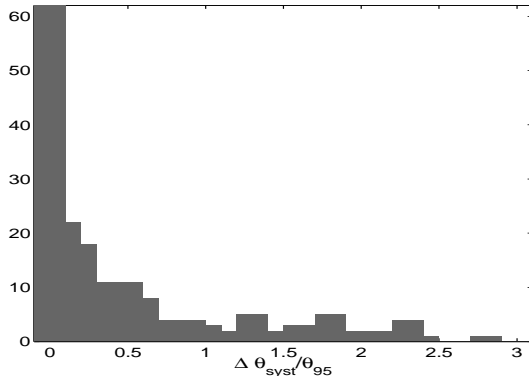


Fig. 12. Histogram of the relative angular separation between the positions found with the Ring and Galprop models in units of the 95% confidence angle for each source.

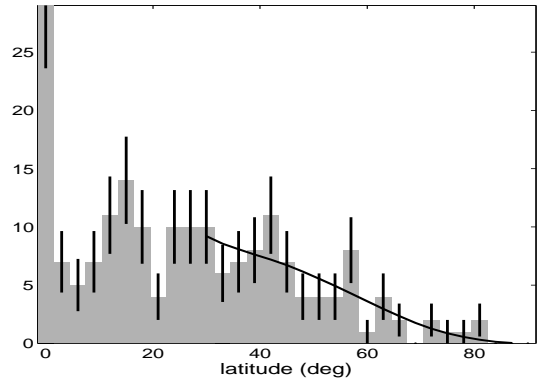


Fig. 14. Latitude distribution of the EGR sources with young Galactic sources at $|b| < 3^\circ$, nearly isotropically distributed sources far from the plane, as expected from the black curve, and a flattening at mid-latitude because of the rapid increase in the interstellar background flux.

Figure 11 and Figure 12 show that, in most cases, the differences are smaller than the statistical uncertainties. The distribution of 95% confidence radii peaks between $\sim 0.2^\circ$ and $\sim 0.7^\circ$. The uncertainty in the background induces an additional systematic error of $\sim 0.2^\circ$ for most sources. It should be kept in mind while looking for counterparts.

We have searched the EGR error circles for potential counterparts of interest such as pulsars from the ATNF catalogue (Manchester et al., 2005), blazar candidates from the ASDC list (Massaro et al., 2005) and the CGRaBS list (Healey et al., 2008), other flat radio sources from the CRATES compilation (Healey et al., 2007), supernova remnants from the Green catalogue (Green, 2006), OB associations (Mel'Nik & Efremov(1995)), and X-ray and TeV pulsar wind nebulae (Li et al. (2008) and Grenier, 2008). The results are displayed in Figure 13. We have found 13 radio pulsar associations in addition to the 6 objects firmly identified by EGRET. Thirteen EGR sources coincide with supernova remnants, 9 with pulsar wind nebulae, 7 with OB associations, 53 with blazar candidates, and 19 with other flat radiosources. These associations should not be considered as identification, but as spatial coincidences worthy of further investigations, in particular with the improved angular resolution of GLAST. Yet, they reveal that as many as 87 sources have no obvious counterpart among the well-known γ -ray emitters despite the large number of pulsars (1775) and radiosources (11 000) that were cross-correlated with the sources and that spread across the entire sky and along the Galactic plane. The lack of blazar counterparts is all the more surprising that the spatial distribution of the sources off the plane is quite reminiscent of an isotropic, therefore extragalactic, distribution. The latitude distribution, shown in Figure 14, is quite consistent above 30° with a sample drawn from a uniform population according to the exposure map, as shown by the black curve. The distribution flattens at lower latitude because of the increased background that drastically limits the survey sensitivity. Studying the consistency with an extragalactic population at medium latitudes and the implication of the lack of a flat radiosource is beyond the scope of this paper and will be addressed in a separate one. The sharp peak below 3° in latitude indicates young emitters. Their clustering in the inner Galaxy ($l \leq 30^\circ$), toward the direction tangent to the Carina arm, and toward the Cygnus region outlines their close relationship to large molecular complexes and star forming regions at a distance of a few kpc.

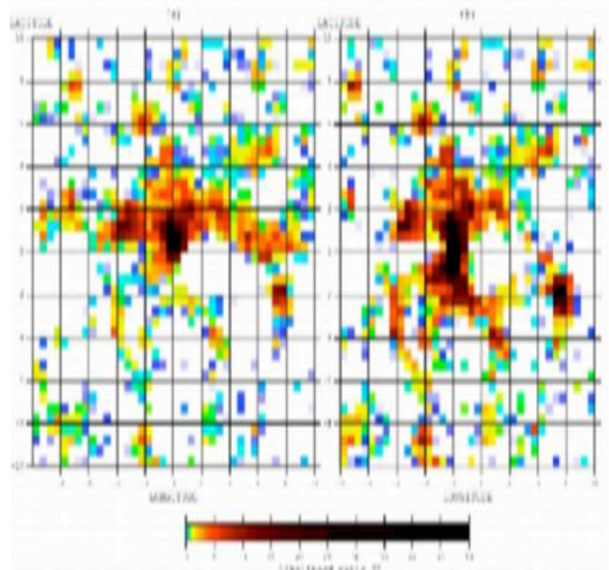


Fig. 15. TS -map obtained at energies above 1 GeV toward the Galactic center above the 3EG (a) and Ring (b) interstellar model

8. Discussion on specific sources

There is considerable interest in the physical processes occurring in the Galactic center region. The 3EG catalogue lists one source located toward the Galactic center, 3EG J1744-3011. We find two point sources in this region, EGR J1740-2851 at $l = -0.55^\circ$, $b = 1.05^\circ$ and EGR J1747-2852 at $l = 0.21^\circ$, $b = -0.24^\circ$. Figure 15 display the TS -map for photons with energies above 1 GeV above the 3EG and the Ring background models. The θ_{95} error radius around EGR J1740-2851 and EGR J1747-2852 formerly excludes the Galactic Center but source locations and fluxes in this direction should be taken with extreme caution since the high gas optical depth around the Galactic center and the velocity pile-up toward the center induce large uncertainties in the total gas column densities.

Coincidences with supernova remnants were noted (Sturmer & Dermer(1995)) and are confirmed in the present analysis (see Table 5), but several also host a pulsar wind nebula, as in CTA 1 and IC 443, so we need much higher

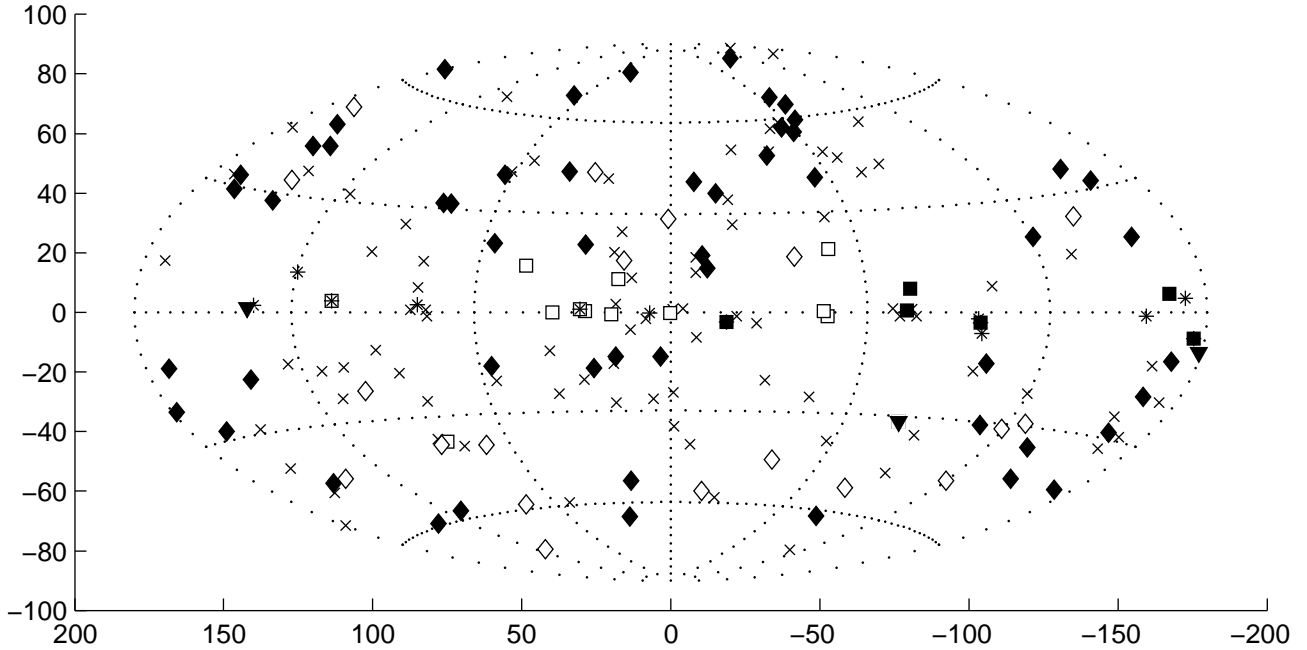


Fig. 13. The revised EGRET source catalog, shown in Galactic coordinates. The symbols indicate the counterpart types found in the error box: identified pulsars as black squares; other ATNF pulsars as open squares; LSI +61 303, LMC, and solar flare as black triangles; ASDC and CGRaBS blazar candidates as black diamonds; other flat-spectrum radio-sources from CRATES as open diamonds; supernova remnants from the Green catalogue as stars; no counterpart as crosses.

Table 5. Names of the sources and supernova remnants found in spatial coincidence

EGRJ0008+7308	G119.5+10.2	CTA1
EGRJ0617+2238	G189.1+3.0	IC443
EGRJ0633+0646	G205.5+0.5	Monoceros
EGRJ1710-4435	G343.0-6.0	RCW114
EGRJ1800-2328	G6.4-0.1	W28
EGRJ1800-2328	G6.5-0.4	
EGRJ1838-0420	G27.8+0.6	
EGRJ1838-0420	G28.8+1.5	
EGRJ2020+4019	G78.2+2.1	γ Cygni
EGRJ2227+6114	G106.3+2.7	
EGRJ0225+6240	G132.7+1.3	HB3

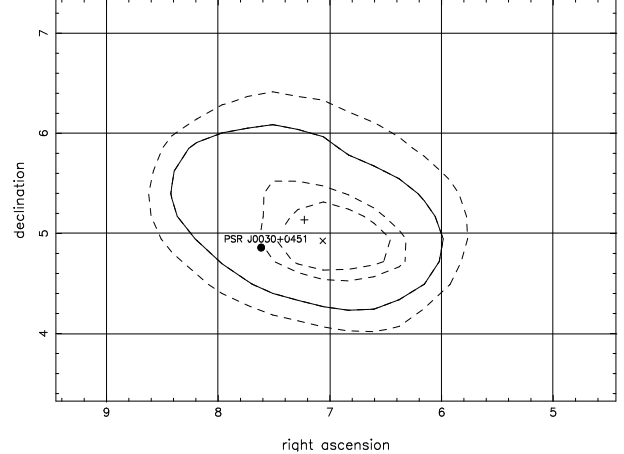


Fig. 16. Likelihood TS contours for energies above 100 MeV and periods encompassing PSR J0030+0451. The cross, the plus sign and the black dot respectively mark the EGR catalog position, the position with maximum likelihood and the pulsar location

resolution γ -ray images to identify the origin of the emission, especially in these crowded regions. EGRET detections are confirmed toward two TeV-emitting wind nebulae around PSR J1420-6048 (in Kookaburra, EGRJ1418-6040) and PSR J1826-1334 (EGRJ1825-1325). Another interesting candidate is the wind nebula of the 11-kyr old and very energetic pulsar PSR J2229+6114 toward EGRJ2227+6114.

We also note, as shown in Figure 16, the positional coincidence within 0.5° between the new EGR J0028+0457 source and the millisecond X-ray pulsar PSR J0030+0451. This 300 pc distant pulsar, discovered in 2000 (Somer, 2000, D'Amico, 2000), has an X-ray counterpart exhibiting a double peaked pulse profile as seen by ROSAT (Becker et al., 2000). Millisecond pulsars have low magnetic fields, they produce relatively few electron-positron pairs so the electric field is not screened and the spectral cutoff due to pair production attenuation occurs at high energy. They are therefore good candidate for accelerating particles to high energies. Harding et al. (2005) has predicted a γ -ray flux for PSR J0030+0451 well above the one of the γ -ray millisecond

pulsar PSR J0218+4232 for which a pulsed emission was marginally detected (Kuiper et al., 2000).

Four massive binaries have been detected at TeV energies, namely PSR B1259-63 (Aharonian et al., 2005), LSI +61° 303 (Albert et al., 2006), LS 5039 (Aharonian et al., 2006)), and Cyg X-1 (Albert et al., 2007), thus illustrating very efficient particle acceleration in compressed or shocked pulsar winds, as well as in microquasar jets. Inverse Compton scattering of the bright stellar radiation would dominate at GeV energies. We find no interesting EGRET counterpart to these high-energy objects, but for the LSI +61° 303 radiosource. The latter had long been associated with the COS-B source 2CG 135+01 and the EGRET

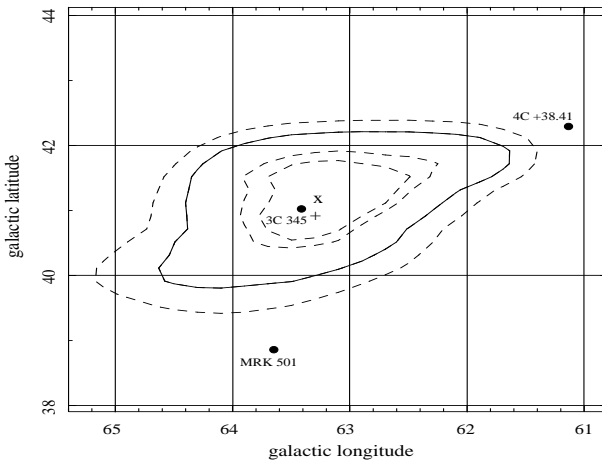


Fig. 17. Likelihood TS contours (50%, 68%, 95% and 99% confidence) for energies above 100 MeV and period 5190. The cross is the EGR catalog position, the plus sign the position with maximum likelihood and the black dots mark the radio positions of 3C345, Mrk 501, and 4C+38.41

source 2EG J0241+6119 (Kniffen et al., 1997), yet it had moved out of the 3EG error box and the marginal γ -ray variability could not be associated with the radio flux variations. In the present analysis, we find the radiosource very near the centre of the EGR J0240+6112 source. On the other hand, we find no source toward the dust enshrouded microquasar candidate, AX J1639.0-4642, or the Be/X-ray binary, AO 0535+26, both proposed as 3EG counterparts (Combi et al., 2003; Romero et al., 2001).

Another noticeable new source is EGR J1642+3940 detected at 5.8σ rather close to 3C345. 3C345 is one of the most prominent flat spectrum ($\alpha = -0.1$) radio-loud, superluminal sources and is therefore an excellent candidate for a γ -ray blazar. EGRET has viewed this region 12 times, in particular during period 5190 when a flare was found. We have analyzed again this particular period with the Ring model since it had not been used in the overall detection search. Figure 17 shows the resulting TS contour for photons with energies above 100 MeV that is well centered on 3C345. The cross corresponds to the EGR position (period 5190), the plus sign to the position with maximum likelihood and the black dots to the position of 3C345 and a nearby AGN. A marginal detection was also obtained for period 3034 at a level of 2.1σ . It should, however, be noted that the small photon excess above 500 MeV has been attributed to a flare from Mrk 501 by Kataoka et al. (1999) because the centroid was closer to the famous TeV source, so the association of EGR J1642+3940 with 3C345 is not clear. GLAST should easily confirm or infirm the association.

Several radiogalaxies (Cen A, NGC 6251, J1737-15) and a Seyfert 1 (GRS 1734-292) had been proposed as possible counterparts to 3EG sources (Hartman et al., 1999; Combi et al., 2003; Foschini et al., 2005; Di Cocco et al., 2004). They triggered some interest because their identification would raise important questions about the origin of the γ rays at large angle from the strongly beamed emission from the jet. We do not, however, confirm the spatial coincidence with EGR sources in the present work. All these galaxies lie well beyond the 95% confidence region of EGR sources.

9. Conclusions

We have searched for point-like sources in the reprocessed EGRET data from cycle 1 to 9 using new interstellar background models based on the most recent *HI*, *CO*, and dark gas data, as well as two different assumptions for the cosmic-ray distribution (the GALPROP diffusion model or a radial emissivity gradient fitted to the diffuse EGRET data). We have used the 3EG tools, likelihood method, procedure and significance threshold to detect sources, but have expanded the search to 3 different energy bands (above 100 MeV, 0.3-1 GeV, and above 1 GeV). The resulting number of detected sources has decreased by more than a third. Many unidentified sources, in particular among those spatially associated with the Gould Belt, are not confirmed as significant excesses. Their emission can be explained by the additional interstellar emission and its structure. Several interesting counterparts to 3EG sources, such as radiogalaxies, massive binaries, and microquasars, are now found outside the 95% confidence region. We have cross-correlated the new source positions with large pulsar, supernova remnant, pulsar wind nebulae, OB associations, and radiosource catalogues, yet half the sample has no attractive counterpart among the potential γ -ray emitters. 30 new possible γ -ray sources have also been found.

This EGR catalog will be available in fits format at the Strasbourg astronomical Data Center (CDS) and in ASCII format at http://www.aim.univ-paris7.fr/EGRET_catalogue/home.html

Acknowledgements. We are deeply grateful to Bob Hartman for his helpful explanations about the construction of the 3EG catalogue, and to Seth Digel and Andy Strong for their help with the gas and Galprop maps.

References

- Aharonian, F., et al. 2005, A&A, 442, 1
- Aharonian, F., et al. 2006, A&A, 460, 743
- Albert, J., et al. 2006, Science, 312, 1771
- Albert, J., et al. 2007, ApJ, 665, L51
- Becker, W., Trumper J., Lommen, A. N., & Backer, D. C. 2000, ApJ, 545, 1015
- Bertin, E., & Arnouts, S. 1996, A&AS, 117, 393
- Combi, J. A., Romero, G. E., Paredes, J. M., Torres, D. F., & Ribó, M. 2003, ApJ, 588, 731
- Combi, J. A., Ribó, M., Mirabel, I. F., & Sugizaki, M. 2004, A&A, 422, 1031
- Dame, T. M., Hartmann, D., & Thaddeus, P. 2001, ApJ, 547, 792
- D'Amico, N. 2000, in Pulsar Astronomy - 2000 and Beyond, 202th ASP Conf. Ser., ed. M. Kramer, N. Wex, & R. Wielebinski (San Francisco: ASP), 27
- Di Cocco, G., et al. 2004, A&A, 425, 89
- Fichtel, C. E., et al. 1994, ApJS, 94, 551
- Finkbeiner, D. P., Davis, M., & Schlegel, D. J. 1999, ApJ, 524, 867
- Foschini, L., et al. 2005, A&A, 433, 515
- Gehrels, N., Macomb, D. J., Bertsch, D. L., Thompson, D. J., & Hartman, R. C. 2000, Nature, 404, 363
- Green D. A. 2006, 'A Catalogue of Galactic Supernova Remnants (2006 April version)', Astrophysics Group, Cavendish Laboratory, Cambridge, United Kingdom
- Grenier, I. A. 1995, Advances in Space Research, 15, 73
- Grenier, I. A. 2000, A&A, 364, L93
- Grenier, I. A. 2004, Cosmic Gamma-Ray Sources, 304, 47
- Grenier, I. A., Casandjian, J.-M., & Terrier, R. 2005, Science, 307, 1292
- Grenier, I. A. 2008, 30th ICRC, Merida, Mexico, in press
- Harding, A.K., Usov, V.V., &Muslimov, A.G. 2005, ApJ, 622, 531
- Hartman, R. C., et al. 1999, ApJS, 123, 79
- Healey, S.E. et al. accepted for publication in ApJS
- Healey, S.E., Romani, R.W., Taylor, G.B., Sadler, E.M., Ricci, R., Murphy, T., Ulvestad, J.S., & Winn, J.N. 2007, Astrophys. J. Suppl., 171, 61-71
- Hermes, W., et al. 2000, Proceedings of the fifth Compton Symposium, 510, 257
- Hunter, S. D., et al. 1997, ApJ, 481, 205
- Kalberla, P. M. W., Burton, W. B., Hartmann, D., Arnal, E. M., Bajaja, E., Morras, R., Pöppel, W. G. L. 2005, A&A, 440, 775

- Kataoka, J., Mattox, J. R., Quinn, J., Kubo, H., Makino, F., Takahashi, T., Inoue, S., Hartman, R. C., Madejski, G. M., Sreekumar, P., Wagner, S. J. 1999, Astroparticle Physics, 11, 149
- Kniffen, D. A., et al. 1997, ApJ, 486, 126
- Kuiper, L., Hermsen, W., Verbunt, F., Thompson, D.J., Stairs, I.H., Lyne, A.G., Strickman, M.S., & Cusumano, G. 2000, A&A, 359, 615
- Lagache, G. 2003, A&A, 405, 813
- Lamb, R. C., & Macomb, D. J. 1997, ApJ, 488, 872
- Li, LX.-H., Lu, LF.-J., Li, LZ., 2007, arXiv:astro-ph/0707.4279v1
- Massaro, E., Sclavi, S., Giommi, P., Perri, M., & Piranomonte, S. 2005, Multifrequency Catalogue of Blazars, Vol. I, Aracne ed-itrice, Roma
- Mattox, J. R., et al. 1996, ApJ, 461, 396
- Manchester, R. N., Hobbs, G. B., Teoh, A. & Hobbs, M. 2005 , M., Astron. J., 129, 1993-2006
- Mel'Nik, A. M., & Efremov, Y. N. 1995, Astronomy Letters, 21, 10
- Moskalenko, I. V., Porter, T. A., & Strong, A. W. 2006, ApJ, 640, L155
- Nolan, P. L., Tompkins, W. F., Grenier, I. A., & Michelson, P. F. 2003, ApJ, 597, 615
- Perrot, C. A., & Grenier, I. A. 2003, A&A, 404, 519
- Pollock, A. M. T., Masnou, J. L., Bignami, G. F., Hermsen, W., Swanenburg, B. N., Kanbach, G., Lichten, G. G., & Wills, R. D. 1981, A&A, 94, 116
- Porter, T. A., & et al. 2005, International Cosmic Ray Conference, 4, 77
- Romero, G. E., Kaufman Bernadó, M. M., Combi, J. A., & Torres, D. F. 2001, A&A, 376, 599
- Schlegel, D. J., Finkbeiner, D. P., & Davis, M. 1998, ApJ, 500, 525
- Somer, A. 2000, in Pulsar Astronomy - 2000 and Beyond, 202th ASP Conf. Ser., ed. M. Kramer, N. Wex, & R. Wielebinski (San Francisco: ASP), 17
- Sowards-Emmerd, D., Romani, R. W., Michelson, P. F., Healey, S. E., & Nolan, P. L. 2005, ApJ, 626, 95
- Sreekumar, P., et al. 1998, ApJ, 494, 523
- Strong, A. W., et al. 1988, A&A, 207, 1
- Strong, A. W., & Mattox, J. R. 1996, A&A, 308, L21
- Strong, A. W., Moskalenko, I. V., & Reimer, O. 2004, ApJ, 613, 962
- Strong, A. W., Moskalenko, I. V., Reimer, O., Digel, S., & Diehl, R. 2004, A&A, 422, L47
- Strong, A. W., Moskalenko, I. V., & Ptuskin, V. S. 2007, Annual Review of Nuclear and Particle Science, 57, 285
- Sturner, S. J., & Dermer, C. D. 1995, A&A, 293, L17
- Thompson, D. J., et al. 1995, ApJS, 101, 259
- Thompson, D. J., et al. 1996, ApJS, 107, 227

Online Material

Table A.1. The EGR catalogue

Num 1	Name EGR J0008+7308	RA 2.01	Dec 73.14	l 119.75	b 10.54	θ_{95} 0.20	F 39.7 63.9 33.4 22.4 48.8 21.6 37.0 44.6 33.1	σ_F 4.4 11.6 9.6 8.7 7.4 7.3 5.3 8.3 9.7	Cnts 330 96 61 37 162 52 212 115 60	\sqrt{TS} 10.9 7.2 4.1 3.0 8.2 3.4 8.5 6.6 4.0	vp p19 p1 p2 p4 p12 p34 p1234 p56 2110	l_{sys} 119.75	b_{sys} 10.54	F_{sys} 41.0	3EG 3EGJ0010+7309	
2	EGR J0028+0457	7.06	4.95	112.15	-57.44	0.51	14.3 7.2 13.9 14.0 7.2 10.7 10.4 24.2 24.7	4.6 4.8 5.9 7.2 4.8 3.3 3.1 11.1 15.6	31 13 20 10 13 43 46 14 6	4.1 1.7 3.0 2.7 1.7 4.0 4.1 2.9 2.3	p34 p1 p3 p4 p12 p1234 p19 3200 3360	112.15	-57.44	14.4		
3	EGR J0039-0945	9.75	-9.75	112.76	-72.38	0.27	13.0 14.6 15.7 14.6 11.0 12.3 22.2 11.5 8.4 9.6 9.1	3.5 5.8 5.4 5.8 4.5 3.6 17.7 3.3 4.6 2.5 2.4	48 23 24 23 22 43 5 73 18 78 74	4.8 3.4 4.0 3.4 3.2 4.5 1.6 4.1 2.1 4.5 4.3	p19 p1 p4 p12 p34 p1234 p789 p12 p1 p2 p19	112.65	-72.40	13.1	3EGJ0038-0949	
4	EGR J0057-7839	14.46	-78.65	-57.47	-38.47	0.53	10.5 11.5 8.4 9.6 9.1	2.7 3.3 4.6 2.5 2.4	73 56 18 78 74	4.6 4.1 2.1 4.5 4.3	p12 p1 p2 p1234 p19	-57.46	-38.44	10.3		
5	EGR J0100+4927	15.01	49.45	124.37	-13.40	0.27	21.5 16.2 10.0 12.5 13.7 12.4 26.4 12.4	6.1 8.3 9.3 3.9 6.2 3.3 22.7 3.2	49 21 8 62 29 87 6 90	4.4 2.3 1.2 3.7 2.5 4.4 1.4 4.4	p1 p3 p4 p12 p34 p1234 p789 p19	123.94	-14.77	12.9		
6	EGR J0117+0254	19.41	2.91	135.83	-59.30	1.15	21.2 14.0 14.0 5.7 5.3	5.9 4.5 4.5 2.7 2.6	37 39 39 29 31	4.6 3.8 3.8 2.3 2.3	p1 p1 p12 p1234 p19	135.83	-59.30	21.1	3EGJ0118+0248	
7	EGR J0141+1719	25.47	17.32	139.75	-43.90	0.85	18.8 8.8 15.6 8.7 11.0 9.3 7.1 15.3 18.3	5.5 4.5 5.2 4.4 3.7 2.8 2.6 6.6 14.8	36 24 30 23 36 56 46 23 6	4.4 2.2 3.8 2.2 3.6 3.8 3.1 2.7 1.4	p1 p1 p3 p12 p34 p1234 p19 210 260	3170	139.52	-43.91	18.4	
8	EGR J0159-3609	29.78	-36.16	-110.71	-73.04	0.59	12.8 4.6 12.4 9.5 34.0 8.7	3.7 3.7 3.6 2.7 26.3 2.5	39 9 38 47 5 47	4.6 1.5 4.5 4.5 1.7 4.3	p1 p4 p12 p1234 p789 p19	-110.85	-73.02	12.9	3EGJ0159-3603	
9	EGR J0204+1505	31.00	15.09	147.75	-44.26	0.48	25.9 3.6 25.7 11.4 10.0 27.5 54.6 4.6	5.7 3.5 5.7 2.9 2.7 6.5 25.6 3.7	68 9 67 72 70 58 11 11	5.8 1.1 5.8 4.7 4.4 5.5 3.0 1.4	p1 p3 p12 p1234 p19 210 260 3170	147.75	-44.27	25.8	3EGJ0204+1458	
10	EGR J0210-5058	32.58	-50.97	-83.84	-61.86	0.14	85.1 83.3 44.1 92.7 66.9 75.2 84.7 77.8 139.9	4.1 6.6 10.6 11.6 9.4 5.6 7.4 4.5 12.7	840 320 48 119 109 371 247 610 202	31.5 18.9 5.7 12.2 10.3 19.5 17.6 25.9 17.7	p19 p1 p2 p3 p4 p12 p34 p1234 p56	-83.82	-61.86	89.7	3EGJ0210-5055	

11	EGR J0216+1128	34.04	11.48	153.74	-46.26	0.98	30.8 17.2 15.7 15.6 4.7 4.4	12.1 4.9 4.8 4.8 2.4 2.3	18 48 44 44 31 33	3.4 4.3 3.9 3.9 2.1 2.1	p789 210 p1 p12 p1234 p19	153.76	-46.29	17.2	3EGJ0215+1123
12	EGR J0223+4300	35.80	43.01	140.25	-16.75	0.21	20.5 13.9 13.2 23.4 19.3 14.8 24.9 18.6 32.7 13.5	2.8 4.0 6.8 5.7 9.3 3.5 5.0 2.9 10.8 6.8	207 58 22 61 16 86 85 172 27 22	9.2 4.1 2.3 5.3 2.6 5.0 6.5 8.0 4.0 2.3	p19 p1 p2 p3 p4 p12 p34 p1234 p789 2110	140.25	-16.75	21.3	3EGJ0222+4253
13	EGR J0238+1659	39.61	16.99	156.47	-38.81	0.34	79.6 52.6 15.6 10.0 52.3 14.0 32.0 29.7 13.8	9.0 6.2 5.1 6.4 6.2 4.0 3.7 3.5 4.8	169 184 39 11 183 50 227 230 34	12.7 11.6 3.8 1.8 11.5 4.3 11.3 11.1 3.6	210 p1 p3 p4 p12 p34 p1234 p19 3170	156.40	-38.78	82.6	3EGJ0237+1635
14	EGR J0240+2812	40.03	28.20	150.28	-28.84	0.55	11.8 13.7 7.9 13.7 13.2 9.4 11.9 20.1 33.7 21.7 11.1	2.4 3.5 4.1 7.5 3.5 3.6 2.5 12.8 11.9 12.7 5.9	116 66 25 16 64 40 109 9 26 9 18	5.7 4.7 2.2 2.1 4.6 3.0 5.6 1.9 3.6 2.4 2.2	p19 p1 p3 p4 p12 p34 p1234 p789 210 36+ 3170	150.26	-28.83	10.9	3EGJ0239+2815
15	EGR J0240+6112	40.12	61.20	135.68	1.06	0.12	81.9 79.4 121.0 59.9 81.9 97.5 68.2 85.1 62.6 121.2	5.4 10.2 13.4 10.5 15.7 8.2 8.7 6.0 12.4 13.4	1000 263 287 179 117 554 301 859 132 288	18.2 9.3 11.4 6.7 6.3 14.7 9.2 17.2 5.8 11.4	p19 p1 p2 p3 p4 p12 p34 p1234 p56 2110	135.57	1.15	85.5	3EGJ0241+6103
16	EGR J0243-5930	40.94	-59.50	-80.08	-52.32	0.95	18.6 9.2 2.4 2.4	6.0 3.4 1.5 1.4	31 31 27 30	4.1 3.3 1.7 1.8	p3 p34 p1234 p19	-80.41	-52.25	18.1	
17	EGR J0253-0336	43.25	-3.61	179.25	-52.65	0.60	16.6 14.3 3.0 2.3 16.4	5.5 4.9 2.1 2.0 5.5	28 29 17 14 27	4.0 3.8 1.6 1.3 3.9	p3 p34 p1234 p19 3170	179.08	-52.55	15.5	3EGJ0253-0345
18	EGR J0328+2147	52.17	21.79	164.73	-28.04	0.48	16.1 13.7 6.2 21.5 7.3 15.6	4.9 4.0 2.5 11.0 2.4 6.9	44 51 58 17 75 22	4.1 4.1 2.8 2.4 3.4 2.8	p3 p34 p1234 p789 p19 3170	164.79	-28.00	16.4	3EGJ0329+2149
19	EGR J0338-0203	54.73	-2.06	-171.80	-42.74	0.36	90.7 5.3 12.3 5.4 41.6 18.1 17.8 9.5 15.6	18.1 3.6 7.3 3.6 7.7 3.6 3.7 4.7 7.7	61 17 13 18 71 90 89 23 16	8.0 1.6 2.0 1.6 7.6 6.3 6.1 2.4 2.5	p4 p1 p3 p12 p34 p1234 p19 210 3170	-171.74	-42.73	87.7	3EGJ0340-0201
20	EGR J0348-5717	57.01	-57.30	-90.40	-46.78	0.63	21.9 4.1 1.4 1.7	7.5 3.2 1.3 1.3	25 10 17 23	4.1 1.5 1.1 1.3	p2 p4 p1234 p19	-90.67	-46.85	23.1	3EGJ0348-5708
21	EGR J0413-1851	63.27	-18.86	-146.07	-43.17	1.26	47.7 12.8 8.4 3.5	15.9 7.4 4.4 2.4	18 12 17 20	4.4 2.2 2.2 1.6	p3290 p3 p34 p1234	-143.25	-42.75	27.4	3EGJ0412-1853

22	EGR J0413-3742	63.40	-37.70	-119.80	-46.58	0.68	3.5 9.1 11.3 8.2 15.6 11.3 9.1 8.6 12.3 6.2 11.6	2.4 2.6 5.0 3.2 9.6 5.0 3.1 2.6 5.2 4.3 4.8	20 57 26 28 9 26 36 54 28 9 23	1.6 4.2 2.6 3.2 2.0 2.6 3.7 4.0 2.8 1.8 3.0	p19 p1234 p1 p3 p4 p12 p34 p19 290 3290 335+	-119.77	-46.55	9.1	
23	EGR J0423+1723	65.94	17.40	178.27	-21.95	0.50	11.8 9.2 21.8 14.4 8.5 17.1 9.1 21.9 26.3 19.0	2.6 3.4 7.2 5.6 3.2 4.4 2.4 10.6 14.3 12.6	170 77 48 42 78 88 148 21 14 12	5.0 3.0 3.5 2.9 2.8 4.4 4.1 2.5 2.2 1.8	p1234 p1 p3 p4 p12 p34 p19 36+ 3170 4130	179.25	-22.12	10.0	3EGJ0423+1707
24	EGR J0425-0032	66.33	-0.54	-165.20	-32.28	0.41	17.6 23.4 21.0 11.3 23.0 9.4 16.3 49.5 13.0	3.0 4.3 12.8 4.6 4.1 4.2 2.9 10.6 7.4	156 107 10 32 115 37 153 51 15	7.1 6.7 2.0 2.9 7.0 2.5 6.8 6.6 2.1	p1234 p1 p2 p4 p12 p34 p19 210 290	-164.98	-32.38	15.0	3EGJ0422-0102
25	EGR J0430+0339	67.58	3.65	-168.48	-28.95	0.51	8.3 6.7 9.0 6.6 6.7 6.9 6.9 14.2 30.3 12.1 21.4	2.3 3.3 6.9 4.5 3.1 3.7 2.4 9.5 14.5 8.5 8.6	104 38 15 21 42 33 77 12 17 10 24	4.0 2.2 1.5 1.6 2.4 2.0 3.2 1.7 2.6 1.7 3.0	p19 p1 p3 p4 p12 p34 p1234 p56 p789 210 4130+	-168.56	-29.08	12.0	3EGJ0429+0337
26	EGR J0433+2906	68.34	29.11	170.47	-12.64	0.17	24.8 6.7 15.7 22.0 28.4 7.2 12.3 10.3 12.4 8.8 37.7	5.2 3.0 11.4 7.7 7.2 2.9 2.6 2.5 8.9 6.8 16.5	126 82 15 52 77 96 226 198 18 21 23	5.4 2.3 1.5 3.2 4.6 2.6 5.2 4.5 1.5 1.4 2.7	p34 p1 p2 p3 p4 p12 p1234 p19 36+ 2+ 4130	170.48	-12.63	27.2	3EGJ0433+2908
27	EGR J0442-0027	70.71	-0.46	-162.61	-28.51	0.50	78.3 21.6 11.2 32.0 11.8	10.1 4.0 2.5 15.2 2.4	139 118 123 14 143	10.8 6.6 5.0 2.8 5.7	p3 p34 p1234 p789 p19	-162.63	-28.51	79.6	3EGJ0442-0033
28	EGR J0450+1145	72.55	11.76	-172.76	-20.29	0.39	101.1 18.4 12.6 9.5 5.6 17.8 6.8 13.1 6.0 11.8 16.0 12.0	18.9 3.6 8.7 5.8 3.9 3.3 3.3 2.4 5.1 2.1 5.7 9.2	69 153 14 27 25 169 49 218 17 248 46 12	7.2 5.9 1.6 1.8 1.5 6.2 2.2 6.2 1.2 6.4 3.3 1.4	36+ p1 p2 p3 p4 p12 p34 p1234 p56 p19 2+ 4130	-172.53	-20.33	94.4	3EGJ0450+1105
29	EGR J0456-2334	74.15	-23.57	-136.15	-35.04	0.69	14.6 6.1 14.6 8.5 8.5 14.7	4.2 5.4 4.2 2.6 2.5 4.2	46 8 46 56 56 46	4.4 1.3 4.4 3.9 3.9 4.4	p1 p4 p12 p1234 p19 290	-135.75	-34.95	14.3	3EGJ0456-2338
30	EGR J0502-0124	75.60	-1.40	-158.96	-24.75	0.36	10.7 10.9 18.5	2.2 3.6 5.8	141 60 47	5.5 3.5 3.8	p1234 p1 p3	-158.96	-24.75	11.3	3EGJ0500-0159

31	EGR J0509+0550	77.41	5.84	-164.70	-19.52	0.44	7.4 9.9 11.5 10.3 8.8 35.3 27.1 8.7 7.3 16.4 11.4 8.2 7.8 8.7 8.1 11.5 11.0 19.9	3.4 3.3 3.0 2.2 6.4 10.4 11.6 1.9 3.0 10.7 5.0 3.5 2.9 2.9 73 140 32 31 9.5	33 61 80 145 15 36 16 180 58 17 37 42 70 73 140 32 31 20	2.4 3.4 4.3 5.5 1.5 4.4 3.2 5.1 2.6 1.7 2.6 2.6 2.9 3.4 4.4 2.3 2.3 2.5	p4 p12 p34 p19 2+ 290 4130 p19 p1 p2 p3 p4 p12 p34 p1234 p56 2+ 4130	-164.70 -19.52 6.6	3EGJ0512-6150
32	EGR J0512-6148	78.14	-61.81	-88.78	-35.29	0.40	6.3 7.1 4.5 8.8 5.5 7.0 5.6	1.7 2.3 4.1 3.4 2.1 2.6 1.6	86 51 10 29 44 39 84	4.5 3.7 1.2 3.1 3.1 3.1 4.1	p1234 p1 p3 p4 p12 p34 p19	-88.83 -35.26 6.6	3EGJ0512-6150
33	EGR J0515+2316	78.96	23.28	-178.92	-8.68	0.49	225.9 16.3 14.0 9.2 6.8 18.7	22.8 3.4 3.2 2.5 2.2 10.4	299 225 213 209 192 22	12.6 5.2 4.7 3.9 3.2 2.0	21 p1 p12 p1234 p19 4130	-179.82 -8.54 168.9	3EGJ0516+2320
34	EGR J0529-3608	82.43	-36.14	-119.43	-31.32	0.69	14.2 16.0 14.0 15.9 13.0 14.1 15.7 24.4 23.2	3.3 5.7 4.5 5.7 4.0 3.3 5.6 6.8 8.5	77 31 39 31 45 77 31 41 21	5.3 3.5 3.8 3.5 3.9 5.3 3.5 4.6 3.6	p1234 p1 p3 p12 p34 p19 290 335+ 3355	-119.08 -31.17 12.9	3EGJ0530-3626
35	EGR J0530+1331	82.71	13.52	-168.64	-11.04	0.16	78.5 98.3 136.2 30.7 89.3 102.4 64.5 86.1 65.4 33.6 136.4 84.3 105.0	3.1 5.3 16.4 7.3 7.2 5.0 5.2 3.6 6.9 18.1 9.3 13.2 16.0	2361 1125 192 127 478 1317 612 1924 381 20 589 123 131	31.1 23.3 10.9 4.7 15.6 25.6 14.9 29.2 11.2 2.1 19.1 8.2 8.3	p19 p1 p2 p3 p4 p12 p34 p1234 p56 36+ 2+ 4130 419+	-168.64 -11.05 79.5	3EGJ0530+1323
36	EGR J0531-2934	82.90	-29.57	-126.68	-29.29	1.00	32.8 9.6 9.9 6.3 6.2 18.1 10.6	11.4 4.8 4.3 2.7 2.7 7.1 8.9	21 19 28 32 32 22 8	4.1 2.5 2.8 p34 p1234 p19 335+ 419+	3355 p3 p1234 p19 335+ 419+	-127.33 -27.00 23.3	3EGJ0531-2940
37	EGR J0534+2159	83.67	21.99	-175.40	-5.77	0.06	230.7 226.6 192.2 197.1 195.6 224.0 201.2 216.9 275.3 255.4 187.9 241.1 136.2 209.5	4.3 6.4 17.8 11.0 10.4 6.0 7.6 4.7 11.3 17.5 22.8 10.6 16.8 28.6	7030 3051 298 789 879 3365 1710 5100 1374 501 171 1150 199 120	75.8 49.4 15.0 24.8 25.7 51.9 36.5 63.6 34.2 20.8 11.2 32.4 10.6 10.2	p19 p1 p2 p3 p4 p12 p34 p1234 p56 p789 36+ 2+ 4130 419+	-175.43 -5.76 230.3	3EGJ0534+2200
38	EGR J0537-6946	84.33	-69.78	-79.73	-31.71	0.39	11.9 9.1 18.8 6.7	2.0 2.6 8.0 6.6	175 74 22 8	7.0 4.1 2.9 1.2	p19 p1 p2 p3	-79.82 -31.76 12.1	3EGJ0533-6916

46	EGR J0722-5121	110.60	-51.36	-97.22	-16.34	0.45	383.3 411.6 9.7 9.1 9.0 5.8 7.8 20.5	20.8 32.5 2.1 4.3 2.8 3.2 2.1 7.2	543 250 107 33 73 31 105 37	30.8 22.0 4.2 3.9 3.7 1.9 4.1 3.4	4130 419+ p1234 p1 p3 p12 p34 p19 3385	-97.02	-16.25	8.2	3EGJ0725-5140
47	EGR J0723+7134	110.86	71.58	143.72	28.15	0.32	19.4 20.3 15.7 10.8 27.6 17.8 16.4 17.4 30.9	1.9 3.4 3.4 4.0 6.8 2.4 3.5 2.0 5.5	358 115 76 37 47 187 84 271 89	13.1 7.5 5.7 3.2 5.4 9.3 5.8 10.9 7.6	p19 p1 p2 p3 p4 p12 p34 p1234 p56 319+	143.71	28.17	19.2	3EGJ0721+7120
48	EGR J0726-4715	111.74	-47.26	-100.78	-13.98	0.50	16.7 15.6 10.1 9.7	3.6 3.4 2.5 2.5	113 114 124 120	5.4 5.2 4.5 4.4	p1 p12 p1234 p19	-100.82	-14.73	17.7	3EGJ0724-4713
49	EGR J0737+1720	114.43	17.34	-157.84	17.84	0.59	13.0 11.6 27.2 15.5 12.0 12.4 13.8 12.6 17.2	2.8 3.5 22.5 6.4 6.5 3.5 4.6 2.8 9.2	97 54 7 22 22 61 35 96 10	5.6 3.9 1.4 3.0 2.2 4.1 3.7 5.5 2.5	p1234 p1 p2 p3 p4 p12 p34 p19 4130	-157.83	17.85	13.1	3EGJ0737+1721
50	EGR J0743+5438	115.87	54.65	163.16	29.20	0.53	24.3 21.5 10.9 7.9 16.9 8.5	4.7 4.3 2.7 2.2 11.2 2.2	82 83 86 79 10 89	6.6 6.3 4.8 4.1 1.9 4.5	227+ p2 p12 p1234 p56 p19	163.13	29.21	23.9	3EGJ0743+5447
51	EGR J0807+4856	121.79	48.94	170.20	32.24	0.59	10.8 10.9 10.7 26.4 10.0 9.9 12.4	2.6 3.5 3.9 24.8 2.4 2.4 4.1	82 47 35 3 88 87 37	5.0 3.7 3.4 1.4 4.9 4.9 3.8	p12 p1 p2 p4 p1234 p19 227+	170.34	32.30	10.8	3EGJ0808+4844
52	EGR J0807+5123	121.86	51.39	167.32	32.49	0.70	9.9 12.9 6.9 8.6 8.6 3.8	2.6 3.6 3.7 2.3 2.3 3.7	81 58 26 84 84 13	4.5 4.3 2.1 4.3 4.3 1.1	p12 p1 p2 p1234 p19 227+	167.12	32.86	10.0	3EGJ0808+5114
53	EGR J0812-0624	123.11	-6.41	-131.70	14.79	0.70	20.6 21.5 129.8 21.5 22.3 14.7 18.1	4.6 5.3 86.1 5.3 5.3 10.3 7.3	73 60 5 60 63 10 25	5.5 5.1 2.4 5.1 5.3 1.7 3.0	p19 p1 p4 p12 p1234 p56 440	-131.77	14.79	18.6	3EGJ0812-0646
54	EGR J0829+0510	127.33	5.18	-140.29	24.10	0.90	17.0 17.0 15.6 15.5 17.1	5.1 5.1 4.8 4.8 10.0	40 40 40 39 13	4.1 4.1 4.0 3.9 2.0	p1 p12 p1234 p19 440	-139.88	24.87	14.4	3EGJ0828+0508
55	EGR J0829+2415	127.46	24.25	-160.14	31.67	0.34	26.5 23.0 16.1 81.3 23.1 31.7 26.5	4.0 5.5 6.0 15.8 5.5 6.0 4.0	118 52 25 49 52 69 118	8.7 5.4 3.4 7.8 5.4 7.2 8.7	p1234 p1 p3 p4 p12 p34 p19	-160.29	31.90	25.3	3EGJ0829+2413
56	EGR J0830+7048	127.57	70.81	143.93	33.57	0.57	8.6 14.7 3.2 9.1 6.6 9.2 8.2 8.9	1.6 3.0 2.5 4.4 6.2 2.0 3.6 1.7	163 96 20 27 7 116 33 148	6.1 6.0 1.4 2.3 1.2 5.4 2.6 5.9	p19 p1 p2 p3 p4 p12 p34 p1234	143.52	34.67	7.8	3EGJ0845+7049

57	EGR J0834-4512	128.70	-45.21	-96.48	-2.88	0.03	6.0 8.8 730.8 699.8 762.6 874.4 727.0 773.2 744.1 91.5 777.6	4.5 4.4 14.5 41.5 19.5 57.5 13.7 18.5 11.0 9.1 23.7	14 26 5101 616 3073 467 5713 3528 9244 186 2154	1.5 2.2 75.5 24.2 58.6 22.7 78.9 62.5 100.8 15.7 49.4	p56 319+ p19 p1 p2 p3 p4 p12 p34 p1234 p789 3385	-96.49	-2.87	785.9	3EGJ0834-4511
58	EGR J0852-1224	133.24	-12.40	-120.77	19.98	0.87	41.2 14.2 14.2 13.5 13.0	11.1 4.4 4.4 4.3 4.3	36 43 43 41 40	5.1 4.0 4.0 3.8 3.7	440 p1 p12 p1234 p19	-121.16	19.39	41.7	3EGJ0852-1216
59	EGR J0853+2015	133.46	20.25	-153.45	35.65	0.30	12.1 10.9 11.4 18.9 10.8 13.7 12.1	3.1 4.5 5.8 7.5 4.5 4.5 3.1	58 27 17 16 27 32 58	4.7 2.9 2.3 3.5 2.9 3.9 4.7	p1234 p1 p3 p4 p12 p34 p19	-153.67	36.00	10.2	3EGJ0853+1941
60	EGR J0901-3525	135.45	-35.42	-100.87	7.26	0.33	25.5 8.4 24.0 8.2 18.7 18.3	4.8 5.6 4.5 5.6 3.6 3.5	146 26 153 25 178 175	6.2 1.6 6.2 1.6 6.0 5.9	p1 p3 p12 p34 p1234 p19	-100.69	7.35	23.7	3EGJ0903-3531
61	EGR J0918+4451	139.52	44.85	175.54	44.29	0.47	14.1 14.1 11.9 19.4 12.8 17.0 14.0 64.5	2.0 3.3 3.4 4.7 2.3 4.1 2.0 62.6	167 64 49 49 111 52 165 2	8.8 5.4 4.3 5.5 6.7 5.5 8.7 1.9	p19 p1 p2 p3 p12 p34 p1234 p789	175.53	44.28	14.1	3EGJ0917+4427
62	EGR J0956+6524	149.24	65.41	146.07	43.06	0.73	13.2 12.1 5.5 4.5 4.6	3.0 2.7 1.7 1.5 1.5	86 95 84 80 85	5.4 5.3 3.7 3.2 3.4	p227+ p2 p12 p1234 p19	146.02	43.05	12.3	3EGJ0958+6533
63	EGR J0957+5513	149.32	55.22	158.85	47.95	0.47	9.7 7.0 9.3 20.0 9.5 8.1 16.7 77.0 9.8 8.8 10.6	1.6 2.5 2.4 5.0 6.7 1.7 4.0 64.3 1.6 2.7 7.0	161 43 65 50 9 107 58 3 164 48 9 1.8	7.3 3.3 4.6 5.1 1.6 5.6 5.2 1.7 7.3 3.8 4180	p1234 p1 p2 p3 p4 p12 p34 p789 p19 p227+ 4180	158.85	47.95	8.5	3EGJ0952+5501
64	EGR J1009+4831	152.39	48.52	167.46	52.19	0.49	5.5 7.6 4.9 7.2 6.2 2.8 5.2 47.3 8.6 7.5 5.7	1.4 2.4 2.4 5.3 1.7 2.5 1.4 34.7 3.1 5.2 4.1	84 45 27 7 72 11 79 4 34 8 11 12	4.5 3.8 2.3 1.6 4.3 p1234 p789 227+ 4180 40	p19 p1 p2 p4 p12 p34 p1234 p789 227+ 4180	167.48	52.18	5.6	3EGJ1009+4855
65	EGR J1021-5831	155.37	-58.53	-75.60	-1.16	0.22	70.5 57.0 51.5 100.7 62.3 57.0 92.0 68.6 83.6 118.3	6.1 8.9 20.2 13.9 22.4 8.1 11.8 6.7 15.3 23.5	1017 361 59 316 62 427 379 796 216 134	12.8 7.0 2.8 8.3 3.1 7.7 8.8 11.3 6.1 5.8	p19 p1 p2 p3 p4 p12 p34 p1234 p56 3385	-75.52	-1.13	81.7	3EGJ1027-5817
66	EGR J1048-5839	162.18	-58.66	-72.46	0.50	0.16	58.0 51.0	5.8 9.2	766 251	11.2 6.1	p19 p1	-72.31	0.28	56.7	3EGJ1048-5840

76	EGR J1222+2845	185.74	28.75	-163.19	83.51	0.23	12.5 4.6 7.6 14.4 26.7 5.9 16.4 11.6 12.1 33.7 7.7 36.7 17.7	1.8 2.5 4.2 3.4 8.9 2.2 3.2 1.9 7.1 11.8 3.7 18.1 5.0	179 22 16 68 28 41 95 149 16 26 21 9 36 36	8.3 2.0 2.2 5.2 4.0 3.1 6.4 7.6 1.9 3.7 2.5 2.8 4.7	p19 p1 p2 p3 p4 p12 p34 p1234 p56 4180 40 2040 virgo3a	-163.19 -163.19	83.51	8.9	3EGJ1222+2841
77	EGR J1225+2115	186.25	21.25	-104.19	81.58	0.07	11.5 9.0 9.2 12.7 10.5 11.7 10.6 11.1 14.4 18.0 30.4 10.7	1.8 3.0 5.3 2.8 2.6 2.3 1.7 10.3 7.6 6.5 14.7 3.7	190 51 22 81 84 99 184 4 20 30 16 35	7.8 3.5 1.9 5.7 4.7 6.1 7.4 1.4 2.2 3.5 2040 3.5	p1234 p1 p2 p3 p12 p34 p19 4180 virgo2 40 2040 virgo3a	-104.19 -104.19	81.58	13.4	3EGJ1224+2118
78	EGR J1229+0203	187.25	2.06	-70.12	64.36	0.26	27.8 19.6 15.9 31.0 24.8 18.4 28.1 23.2 56.2 9.6 15.7 33.8	1.9 3.4 5.1 3.9 4.7 2.9 3.0 2.1 6.3 7.6 5.2 4.9	771 155 53 202 107 207 305 513 241 13 52 152	17.5 6.6 3.5 9.9 6.5 7.5 11.6 13.4 11.6 1.4 3.5 8.9	p19 p1 p2 p3 p4 p12 p34 p1234 p56 p789 virgo2 virgo3a	-70.12 -70.12	64.36	26.5	3EGJ1229+0210
79	EGR J1231-1412	187.86	-14.20	-64.38	48.39	0.25	8.3 4.0 15.4 6.9 8.4 3.8 6.8 17.6 22.4 26.7	1.6 2.6 4.0 3.4 2.3 2.5 1.7 4.7 5.7 10.1	170 23 63 25 83 25 111 58 54 23	6.0 1.7 4.6 2.3 4.2 1.7 4.5 p1234 4.6 5.1 3.3	p19 p1 p2 p4 p12 p34 p1234 p56 virgo2 2040	-64.38 -64.38	48.39	9.1	3EGJ1234-1318
80	EGR J1237+0434	189.31	4.58	-66.23	67.20	0.66	9.2 10.2 14.3 5.5 9.3 11.4 6.7 9.0 10.7 14.4 15.2 5.3	1.4 2.7 4.4 2.7 3.5 2.3 2.1 1.6 4.5 4.4 6.8 3.4	249 81 46 37 40 126 73 199 41 46 18 24	7.3 4.5 4.0 2.2 3.2 5.9 3.5 6.7 2.7 4.0 2.8 1.7	p19 p1 p2 p3 p4 p12 p34 p1234 p56 virgo2 2040 virgo3a	-66.01 -66.01	67.15	9.7	3EGJ1236+0457
81	EGR J1247-0733	191.75	-7.55	-59.00	55.31	0.24	8.1 14.0 4.9 10.9 7.4 7.0 14.2	1.7 4.1 3.3 2.9 1.9 3.9 8.8	219 91 19 114 143 43 19	5.2 3.8 1.7 4.2 4.3 1.9 1.8	p19 p1 p2 p12 p1234 p56 p789	-59.17 -59.17	55.03	8.9	3EGJ1246-0651
82	EGR J1256-0552	194.01	-5.87	-54.96	56.98	0.09	83.7 161.7 6.2 41.9 22.2 104.5 30.5 70.7 110.9 132.4 6.0 43.6	2.5 6.6 3.5 5.0 3.9 4.5 3.1 2.8 5.9 13.5 3.9 6.0	2388 1104 24 176 121 1114 294 1434 755 189 18 128	47.2 37.3 2.0 11.3 7.2 34.1 12.7 35.9 26.8 14.6 1.7 9.9	p19 p1 p2 p3 p4 p12 p34 p1234 p56 p789 virgo2 virgo3a	-54.96 -54.96	56.98	86.4	3EGJ1255-0549

83	EGR J1259-2209	194.92	-22.16	-54.55	40.67	0.58	8.6 9.6 3.2 20.4 8.9 6.2 12.2 8.0 13.5 17.9 26.6	2.0 3.7 3.0 8.2 4.3 2.4 3.9 2.0 7.5 11.4 10.0	128 43 15 23 27 58 51 108 19 9 24	4.9 3.0 1.1 3.1 2.4 2.9 3.7 4.5 2.1 2.0 3.4	p19 p1 p2 p3 p4 p12 p34 p1234 p56 2040 virgo3a	-54.63	40.60	8.0	
84	EGR J1309-0535	197.29	-5.59	-48.96	57.00	0.32	6.9 12.1 5.1 4.2 6.1 9.9 5.0 7.6 7.5 6.9 9.2	1.6 3.8 3.2 3.8 2.9 2.7 2.3 1.8 3.5 3.8 6.2	189 78 19 16 34 100 47 149 48 20 10	4.9 3.5 1.8 1.2 2.3 4.1 2.3 4.7 2.3 2.1 1.8	p19 p1 p2 p3 p4 p12 p34 p1234 p56 virgo2 2040	-48.28	57.28	7.9	3EGJ1310-0517
85	EGR J1314-3417	198.58	-34.30	-51.70	28.33	0.45	12.6 15.8 15.9 8.9 15.6 6.3 12.6	2.3 4.6 3.9 5.2 3.0 3.5 2.3	156 58 78 17 134 24 156	6.3 4.1 4.8 2.0 6.2 2.0 6.3	p1234 p1 p2 p4 p12 p34 p19	-51.69	28.20	13.1	3EGJ1314-3431
86	EGR J1328-4337	202.07	-43.62	-50.04	18.75	0.37	10.5 5.1 14.4 10.3 7.2 10.5 10.0 10.5 15.9	2.5 4.2 4.4 5.1 6.2 3.1 4.0 2.5 7.6	144 23 64 29 14 94 48 144 22	4.8 1.3 3.7 2.3 1.2 3.8 2.8 4.8 2.4	p1234 p1 p2 p3 p4 p12 p34 p19 314+	-50.04	18.75	10.8	3EGJ1324-4314
87	EGR J1337-1310	204.45	-13.17	-40.02	48.16	0.63	30.2 15.2 9.3 10.5 2.6 38.2 7.2 5.4 23.8 17.6	6.5 8.9 3.5 3.3 1.8 20.3 1.9 5.0 10.3 8.0	82 14 43 58 36 12 124 9 16 19	5.7 2.0 3.0 3.7 1.5 2.3 4.3 1.2 3.1 2.7	p56 p3 p4 p34 p1234 p789 p19 virgo2 2040 virgo3a	-39.34	47.22	26.5	3EGJ1339-1419
88	EGR J1338+5102	204.54	51.04	105.73	64.50	0.46	8.5 4.3 18.4 13.6 7.9 11.4 8.4 6.0	2.5 2.7 6.9 8.0 2.7 7.5 2.5 3.8	50 17 23 9 42 8 50 12	4.0 1.8 3.6 2.2 3.5 1.9 4.0 1.9	p1234 p1 p2 p4 p12 p34 p19 p19	105.73	64.50	7.8	3EGJ1337+5029
89	EGR J1345+2912	206.33	29.20	45.98	77.95	0.73	9.9 11.8 6.2 10.6 5.6 8.3 39.6 20.9	2.6 3.8 5.1 3.4 3.9 2.6 16.5 6.8	61 30 9 35 14 47 14 24	4.7 4.0 1.4 3.8 1.6 3.9 3.4 4.1	p19 p1 p3 p12 p34 p1234 p56 40	46.62	77.52	10.6	3EGJ1347+2932
90	EGR J1409-0736	212.27	-7.61	-25.88	50.50	0.25	107.2 6.8 5.4 43.9 3.8 26.2 24.6 28.7 99.6 78.6	9.6 4.1 3.4 4.5 3.1 2.9 2.8 15.5 12.7 18.3	234 27 22 268 18 283 292 14 115 35	16.7 1.8 1.7 12.9 1.3 11.2 11.0 2.2 11.8 6.3	p2 p1 p4 p12 p34 p1234 p19 250 virgo2 2040	-25.89	50.50	100.8	3EGJ1409-0745
91	EGR J1414-6224	213.50	-62.41	-47.67	-1.05	0.35	81.8 83.4 75.5 25.5	12.7 14.2 28.8 13.6	358 300 58 85	7.0 6.4 2.9 1.9	p12 p1 p2 p3	-47.46	-0.42	86.5	3EGJ1410-6147

92	EGR J1418-6040	214.72	-60.68	-46.56	0.40	0.22	38.4 29.2 51.7 49.9 79.8 28.2 68.7 20.0 64.7 73.5 15.3 43.7 42.9 53.7 59.5	17.1 10.6 8.2 8.1 24.4 15.3 11.9 13.3 15.1 19.2 12.0 8.5 8.5 24.3 17.2	76 156 502 484 88 74 369 76 218 147 71 439 431 63 152	2.4 2.9 6.7 6.5 3.6 1.9 6.2 1.5 4.5 4.1 1.3 5.4 5.3 2.3 3.7	p4 p34 p1234 p19 230 314+ p34 p1 p3 p4 p12 p1234 p19 230 314+	-46.32	0.38	58.1	3EGJ1420-6038	
93	EGR J1424+3730	216.08	37.50	66.73	67.89	0.85	17.6 10.2 9.5 9.4	5.1 3.7 3.7 3.7	33 30 28 27	4.6 3.4 3.1 3.1	p1 p12 p1234 p19	67.37	67.80	17.6	3EGJ1424+3734	
94	EGR J1428-4240	217.16	-42.67	-38.65	16.70	0.62	26.3 6.7 25.3 29.0 3.7 11.3 11.2 38.8	5.1 4.1 7.0 7.6 3.0 2.7 2.6 20.1	118 28 62 60 29 141 139 14	6.2 1.8 4.4 4.7 1.3 4.8 4.7 2.4	p34 p1 p3 p4 p12 p1234 p19 4235	-37.80	17.68	23.1	3EGJ1429-4217	
95	EGR J1458-1904	224.56	-19.07	-20.00	34.52	0.59	19.9 7.9 13.1 9.6 9.5 33.5 14.5	5.2 6.7 3.9 3.1 3.1 15.4 11.8	58 9 61 62 61 12 6	4.7 1.3 3.9 3.5 3.4 3.0 1.5	p1 p4 p12 p1234 p19 250 4235	-20.30	34.39	19.8	3EGJ1457-1903	
96	EGR J1504-1539	226.14	-15.65	-16.04	36.40	0.65	37.5 36.4 21.4 6.6 6.4	10.6 10.5 6.6 3.1 3.1	32 31 38 38 37	4.9 4.8 4.2 2.3 2.3	p3 p34 p1234 p19	3390	-15.97	36.40	38.0	3EGJ1504-1537
97	EGR J1512-0857	228.13	-8.95	-8.66	40.30	0.40	18.7 22.9 15.9 14.9 21.9 14.3 18.5 16.7	3.7 5.1 7.9 7.2 5.1 5.3 3.7 8.0	112 83 19 17 81 33 111 20	6.0 5.5 2.4 2.5 5.2 3.3 6.0 2.5	p1234 p1 p3 p4 p12 p34 p19 3390	-8.64	40.32	20.4	3EGJ1512-0849	
98	EGR J1516-2536	229.18	-25.60	-20.34	26.72	0.69	28.6 4.6 6.7 4.8 17.6 8.1 7.6 25.1 32.9 28.8	8.3 3.7 5.0 3.0 5.8 2.7 2.6 19.8 19.3 13.2	41 17 20 32 44 75 71 10 12 14	4.4 1.3 1.5 1.7 3.6 3.4 3.2 1.5 2.0 2.9	p3 p1 p2 p12 p34 p1234 p19 2260 3023 3390	-20.11	27.10	27.5	3EGJ1517-2538	
99	EGR J1607+8216	241.84	82.27	116.06	32.03	0.60	9.8 10.8 8.8 6.1 8.6 8.4 11.1	2.5 3.0 4.9 6.0 2.2 2.2 4.1	73 59 17 7 79 77 34	4.6 4.4 2.0 1.1 4.5 4.4 3.2	p12 p1 p2 p3 p1234 p19 220	115.97	32.03	9.5	3EGJ1621+8203	
100	EGR J1607+1533	241.99	15.55	29.10	43.10	0.60	39.3 11.1 19.4 8.4 16.6 10.8 10.5 20.6	12.2 4.9 9.3 4.5 8.4 4.0 4.0 9.5	27 29 15 24 14 40 39 15	4.3 2.6 2.6 2.1 2.5 3.1 3.0 2.8	250 p1 p3 p12 p34 p1234 p19 3390	29.55	43.87	39.5	3EGJ1605+1553	
101	EGR J1608+1051	242.04	10.85	23.37	41.09	0.39	27.5 27.1 20.4 20.4 29.1	5.2 5.2 4.2 4.2 11.0	93 92 90 90 22	6.6 6.6 5.9 5.9 3.4	p1 p12 p1234 p19 250	23.37	41.09	31.5	3EGJ1608+1055	
102	EGR J1609-1128	242.32	-11.47	0.82	28.44	0.75	83.8	27.4	24	4.2	229+	0.82	28.44	82.1	3EGJ1607-1101	

103	EGR J1615+3426	243.90	34.44	55.52	46.00	0.16	22.3 25.6 4.7 48.1 64.1 79.2 22.3 74.8 30.1 19.2	9.6 3.2 3.7 8.1 28.6 16.5 4.1 14.3 4.1 5.1	28 189 12 83 10 47 93 55 148 44	2.7 10.7 1.4 8.3 3.4 7.1 7.0 7.7 9.9 4.9	p2 p19 p1 p2 p3 p4 p12 p34 p1234 p56	55.53	46.01	25.9	3EGJ1614+3424
104	EGR J1617-2610	244.28	-26.17	-9.78	17.28	0.90	136.6 21.0 17.4 36.5 8.2 26.3 14.0 12.3 15.0 41.6 43.9	32.9 8.1 9.1 12.7 4.6 7.6 4.0 3.9 11.5 15.6 25.3	62 73 45 75 77 122 197 183 22 42 18	5.1 2.8 2.0 3.1 1.8 3.7 3.7 3.3 1.4 3.0 1.9	4230 p2 p3 p4 p12 p34 p1234 p19 50 2260 3390	-9.82	17.16	107.9	3EGJ1612-2618
105	EGR J1619+2223	244.75	22.39	39.11	42.96	1.23	38.6 21.5 21.1 8.0 13.5 44.4 16.1 26.8 19.5 49.6 41.3 35.6 17.9 25.8 43.2 37.1	13.3 3.4 5.1 6.6 8.2 10.5 4.1 6.6 3.5 15.7 31.3 20.5 13.2 21.6 28.3 16.4	22 342 131 29 38 104 159 137 292 47 9 16 18 11 15 31	4.0 6.9 4.5 1.3 1.7 4.9 4.3 4.5 6.1 3.8 2.230 2.1 1.5 3.3 1.3 4.210 2.5	p56 p19 p1 p2 p3 p4 p12 p34 p1234 p56 2230 229+ 3023 3390 4210 4235	39.05 -7.23	42.94 16.30	32.7 26.8	3EGJ1626-2519
106	EGR J1625-2505	246.26	-25.09	-7.69	16.69	0.25	21.5 21.1 8.0 13.5 44.4 16.1 26.8 19.5 49.6 41.3 35.6 17.9 25.8 43.2 37.1	3.4 5.1 6.6 8.2 10.5 4.1 6.6 3.5 15.7 31.3 20.5 13.2 21.6 28.3 16.4	342 131 29 38 104 159 137 292 47 9 16 18 11 15 31	4.0 4.5 1.3 1.7 4.9 4.3 4.5 6.1 3.8 2.230 2.1 1.5 3.3 1.3 4.210 2.5	p56 p19 p1 p2 p3 p4 p12 p34 p1234 p56 2230 229+ 3023 3390 4210 4235	-11.10	13.15	258.5	3EGJ1625-2955
107	EGR J1625-2958	246.49	-29.97	-11.29	13.26	0.26	255.5 12.0 13.4 5.9 120.4 43.0 74.1 45.7 289.5 81.1 21.4 226.2 242.6	15.0 6.1 7.0 3.4 8.2 3.6 14.0 3.5 35.8 32.3 11.9 34.2 23.1	612 48 36 60 615 662 98 763 142 20 24 100 223	25.0 2.1 2.1 1.8 19.7 14.3 6.7 15.8 11.6 3.2 2.0 9.3 15.7	p4 p2 p3 p12 p34 p1234 p56 p19 4230 2230 2260 4210 4235	-11.10	13.15	258.5	3EGJ1625-2955
108	EGR J1635+3825	248.95	38.43	61.50	42.25	0.24	48.3 103.3 31.8 43.1 39.5 68.6 39.5 62.8 26.3 40.9	3.7 9.2 6.8 24.1 11.7 5.8 10.5 5.1 5.1 21.0	428 235 66 9 33 299 41 339 85 10	18.3 17.3 6.2 2.4 4.6 17.1 5.1 17.6 6.6 2.6	p19 p1 p2 p3 p4 p12 p34 p1234 p56 p789	61.50	42.25	46.8	3EGJ1635+3813
109	EGR J1638-5157	249.61	-51.95	-25.98	-3.34	0.45	61.5 10.8 18.4 28.1 20.2 62.0 22.3 17.1 84.1 53.2 34.9	13.9 9.2 14.8 7.7 6.2 30.2 6.0 15.9 61.9 29.8 33.3	142 43 30 177 195 32 226 21 12 28	5.0 1.2 1.3 3.9 3.4 2.3 3.9 1.1 1.5 2.0	p2 p1 p4 p12 p1234 p56 p19 50 2230 2260 4235	-25.78	-3.35	46.0	3EGJ1638-5155
110	EGR J1640-2807	250.17	-28.13	-7.70	12.06	0.43	19.8 11.5 20.1 17.2 9.0 18.7 9.5	5.2 5.7 6.6 8.1 2.8 11.5 2.7	133 50 80 47 158 26 181	4.2 2.2 3.4 2.3 3.4 1.8 3.7	p34 p2 p3 p4 p1234 p56 p19	-7.67	12.01	17.9	3EGJ1638-2749

118	EGR J1732-3126	263.06	-31.44	-3.66	1.11	0.25	19.3 14.1 17.8 13.8 13.3 21.0 29.0 34.8 29.0 23.7 44.2 48.8 27.0 45.5 34.3 43.9 31.0 50.2 25.0 79.6	5.8 6.0 5.6 5.5 3.4 8.7 8.6 5.9 10.4 12.5 11.8 15.9 8.0 9.5 6.1 21.9 13.5 22.8 24.1 41.1	62 39 62 46 109 30 50 815 197 122 277 159 322 433 736 86 121 82 35 40	3.8 2.7 3.7 2.8 4.3 2.9 4.1 6.1 2.9 1.9 3.9 3.2 3.5 5.0 5.8 2.1 2.4 2.3 1.1 2.1	p1 p3 p12 p34 p19 330+ 200 p19 p1 p2 p3 p4 p12 p34 p1234 p56 50 330+ 2260 4235	-3.57	1.09	40.4	3EGJ1734-3232
119	EGR J1734-1315	263.55	-13.26	12.02	10.48	0.23	28.1 14.7 41.1 30.7 43.9 22.6 33.7 27.7 34.6 19.3 23.6 47.3 40.1 54.8 30.1 44.6 136.0 29.8 77.9 96.1	3.1 4.7 8.9 5.8 9.3 4.3 4.9 3.2 10.3 8.7 8.0 17.9 14.3 31.7 16.2 19.2 45.5 14.8 31.2 33.0	593 104 126 195 112 229 300 526 72 43 67 32 40 14 23 30 31 30 27 40	10.3 3.4 5.3 6.0 5.6 5.8 7.9 9.6 3.8 2.4 3.3 3.2 3.2 2.2 2.1 2.7 3.8 3.0 3.8	p19 p1 p2 p3 p4 p12 p34 p1234 p56 50 330+ 4230 200 2230 2260 229+ 2310 3023 4210 4235	12.01	10.52	31.9	3EGJ1733-1313
120	EGR J1740+4946	265.09	49.77	76.72	31.57	0.86	21.5 17.1 9.9 14.6 10.5 8.0	6.2 10.8 3.6 9.8 3.4 2.8	45 12 50 13 62 61	4.3 1.8 3.1 1.7 3.5 3.1	p1 p3 p12 p34 p1234 p19	76.63	31.49	23.7	
121	EGR J1740+5213	265.19	52.22	79.60	31.73	0.37	26.3 41.0 15.0 14.0 12.0	5.7 27.5 3.6 3.3 2.9	76 6 83 90 95	6.0 2.0 5.1 5.1 4.9	p2 p4 p12 p1234 p19	79.53	31.78	26.9	3EGJ1738+5203
122	EGR J1743-1002	265.94	-10.04	16.05	10.11	0.63	37.4 12.1 24.2 14.5 6.7 10.8 21.0 11.3 56.8 47.1	10.4 5.3 10.5 4.7 3.3 3.1 10.5 11.3 37.1 20.9	89 82 52 130 117 213 38 16 12 28	4.0 2.4 2.5 3.3 2.1 3.6 2.2 1.1 1.9 2.6	p56 p1 p2 p12 p1234 p19	16.34	9.64	29.0	3EGJ1746-1001
123	EGR J1758-3923	269.62	-39.40	-7.71	-7.58	0.98	83.5 19.1 11.1 25.9 3.9 28.4 42.3 40.9	18.2 5.9 4.6 13.9 2.7 25.8 22.0 19.8	83 103 88 27 75 10 18 25	5.5 3.5 2.5 2.1 1.5 1.2 2.3 2.4	330+ p3 p34 p56 p19 2230 2260 3023	-8.65	-8.43	72.4	3EGJ1800-3955
124	EGR J1800-2328	270.20	-23.48	6.43	-0.16	0.23	59.2 63.0 34.4 48.6 94.4 53.1 60.5 56.3 126.0	6.3 11.3 14.7 11.1 17.7 9.0 9.4 6.5 27.2	1421 454 145 382 295 606 664 1260 203	9.8 5.9 2.4 4.5 5.7 6.2 6.7 9.1 5.0	p19 p1 p2 p3 p4 p12 p34 p1234 p56	6.40	-0.25	60.0	3EGJ1800-2338

125	EGR J1809-2322	272.42	-23.37	7.52	-1.88	0.16	55.5 67.0 124.2 40.3 39.6 59.9 103.4 97.8 177.7 43.2 38.8 70.5 38.4 32.5 49.5 35.6 42.3 80.0 35.6 50.2 47.6 80.8 96.1 102.9 64.0	15.1 18.6 31.2 28.6 35.2 53.8 32.8 44.5 61.7 5.4 9.7 14.0 9.3 14.2 8.0 7.8 5.6 24.4 12.8 15.2 43.0 27.6 33.1 45.9 52.1	212 198 125 42 30 20 103 50 1007 273 275 303 99 541 390 925 115 133 156 18 76 69 41 15	3.9 3.8 4.4 1.5 1.2 1.2 3.4 2.4 3.3 8.4 4.2 5.4 4.3 2.4 6.6 4.8 8.0 3.5 2.9 3.5 1.2 3.2 3.2 2.5 1.3	50 330+ 4230 2260 229+ 2310 3023 4210 4235 p19 p1 p2 p3 p4 p12 p1234 p56 50 330+ 2230 2260 229+ 2310 4235	7.54	-1.78	58.0	3EGJ1809-2328
126	EGR J1812-1316	273.04	-13.27	16.66	2.47	0.22	45.6 44.7 44.2 40.5 58.3 45.6 46.5 42.9 44.1 44.9 86.8 64.2 89.8 59.1 34.7 83.4	5.5 8.8 14.4 9.2 16.0 7.5 8.0 5.2 15.6 12.7 29.0 30.5 33.2 38.2 29.4 52.4	923 350 119 300 133 481 450 970 103 171 65 40 54 26 25 22	8.9 5.4 3.3 4.6 4.0 6.5 6.2 8.8 3.0 3.8 3.4 2.3 3.0 1.7 1.2 1.8	p1234 p1 p2 p3 p4 p12 p34 p19 50 330+ 4230 2260 229+ 2310 3023 4210	16.76	2.29	46.2	3EGJ1812-1316
127	EGR J1814+2932	273.59	29.54	56.52	20.46	0.80	17.3 7.0 5.8 6.4 22.5 15.8 10.7	4.8 3.1 2.7 2.7 8.6 7.5 8.0	63 45 49 55 25 24 14	4.3 2.5 2.3 2.6 3.2 2.5 1.5	p1 p12 p1234 p19 p20 p19 328+	56.99	20.79	17.8	
128	EGR J1814-6423	273.64	-64.39	-29.98	-20.46	0.41	14.6 17.4 19.1 13.9 15.7 11.9 14.5	3.9 5.8 8.8 8.7 4.7 7.1 3.9	66 40 18 12 51 15 65	4.5 3.7 2.8 1.9 4.0 2.0 4.4	p1234 p1 p2 p3 p12 p34 p19	-29.97	-20.43	15.5	3EGJ1813-6419
129	EGR J1820-7920	275.16	-79.35	-45.39	-25.22	0.44	24.4 22.2 27.0 20.2 18.8 18.7	5.8 6.6 11.5 10.2 4.4 4.4	63 40 21 16 74 73	5.3 4.3 2.9 2.4 5.2 5.2	p12 p1 p2 p3 p1234 p19	-45.40	-25.24	23.3	3EGJ1825-7926
130	EGR J1822+1654	275.56	16.91	45.03	13.93	0.60	36.3 32.1 23.6 6.4 6.6 35.5	10.8 9.9 8.6 3.7 3.8 23.4	42 50 43 39 41 9	4.2 3.8 3.2 1.8 1.9 1.9	328+ p3 p34 p1234 p19 3315	44.95	13.90	39.7	3EGJ1822+1641
131	EGR J1825-1325	276.41	-13.43	18.07	-0.50	0.33	83.5 38.0 143.9 101.7 93.1 69.1 99.3 83.2 100.7 53.3 114.0	8.8 14.1 28.1 15.4 27.5 12.6 13.5 9.2 27.6 25.6 21.1	1840 307 307 753 201 707 950 1645 228 122 453	9.8 2.7 5.4 6.8 3.5 5.6 7.6 9.3 3.8 2.1 5.6	p19 p1 p2 p3 p4 p12 p34 p1234 p56 50 330+	18.11	-0.50	145.6	3EGJ1826-1302

132	EGR J1832-2052	278.04	-20.88	12.17	-5.31	0.36	150.4	47.5	107	3.3	4230				
							96.1	26.4	211	3.8	200				
							329.5	59.1	178	6.2	229+				
							184.7	55.2	111	3.5	3023				
							273.8	91.7	67	3.3	4210				
133	EGR J1835+5919	278.86	59.33	88.75	25.08	0.13	17.7	3.4	392	5.6	p19	12.10	-5.40	20.0	3EGJ1832-2110
							11.5	5.5	90	2.2	p1				
							32.7	10.1	99	3.6	p2				
							18.5	5.7	140	3.4	p3				
							19.3	9.7	48	2.1	p4				
							17.0	4.8	186	3.7	p12				
							18.6	4.9	186	4.0	p34				
							17.7	3.5	370	5.4	p1234				
							25.2	14.7	32	1.8	p56				
							22.2	8.8	75	2.7	330+				
							91.3	24.4	60	4.6	2260				
							39.2	22.7	25	1.9	3023				
							39.1	26.5	15	1.7	4210				
134	EGR J1837-0557	279.35	-5.95	26.04	0.40	0.19	69.2	4.3	556	23.1	p19	88.75	25.08	69.4	3EGJ1835+5918
							58.0	7.6	131	10.8	p1				
							68.3	6.1	284	16.1	p2				
							76.7	12.7	76	9.0	p3				
							65.3	4.8	420	19.6	p12				
							77.3	12.7	79	9.1	p34				
							66.5	4.5	495	21.4	p1234				
							100.2	17.9	58	8.5	p789				
135	EGR J1838-0420	279.60	-4.34	27.58	0.91	0.71	72.2	12.5	461	6.1	p34	25.77	0.31	46.8	3EGJ1837-0606
							24.2	10.7	182	2.3	p1				
							64.8	13.8	333	4.9	p3				
							98.9	28.6	123	3.7	p4				
							22.0	10.0	187	2.2	p12				
							43.2	7.8	643	5.7	p1234				
							41.5	20.8	102	2.1	p56				
							43.1	7.3	747	6.1	p19				
							68.5	17.5	228	4.1	330+				
							55.9	50.8	22	1.1	4230				
							29.3	15.6	104	1.9	200				
							140.6	87.5	20	1.8	430				
136	EGR J1847-3220	281.85	-32.34	3.18	-13.34	0.35	369.1	71.8	121	5.9	4230	27.44	1.06	310.4	3EGJ1837-0423
							14.9	13.0	110	1.1	p1				
							83.3	34.7	94	2.5	p4				
							14.5	12.3	121	1.2	p12				
							23.4	15.1	140	1.6	p34				
							19.6	9.5	280	2.1	p1234				
							44.3	26.2	110	1.7	p56				
							23.0	9.0	387	2.6	p19				
							40.1	19.0	150	2.2	200				
							8.2	5.2	83	4.4	p2	3.21	-13.30	25.4	3EGJ1847-3219
							4.5	3.0	80	3.0	p12				
							4.2	2.2	81	2.2	p1234				
							21.1	13.5	14	1.8	2260				
							35.5	18.8	14	2.4	2310				
							15.8	15.1	8	1.2	3023				
137	EGR J1856+0235	284.23	2.59	35.86	-0.04	0.52	165.4	33.5	192	5.4	p56	34.54	-0.71	208.2	3EGJ1856+0114
							51.1	48.5	20	1.1	p2				
							31.2	15.6	118	2.0	p3				
							96.2	42.0	49	2.5	p4				
							42.8	14.7	183	3.0	p34				
							9.0	8.4	105	1.1	p1234				
							22.7	8.3	292	2.8	p19				
							34.3	20.4	78	1.7	330+				
							128.9	87.1	19	1.6	430				
138	EGR J1912-2000	288.06	-20.01	17.08	-13.41	0.44	14.3	2.6	239	6.2	p1234	17.12	-13.37	17.4	3EGJ1911-2000
							14.1	3.9	99	4.0	p1				
							8.8	5.9	23	1.6	p2				
							18.1	4.6	104	4.4	p3				
							11.8	9.4	16	1.4	p4				
							12.7	3.3	122	4.3	p12				
							18.1	4.2	130	4.8	p34				
							13.7	2.6	232	6.0	p19				
							15.9	6.7	45	2.6	330+				
							35.2	19.0	16	2.2	4230				
							11.1	8.3	15	1.5	200				
							27.4	22.3	8	1.4	430				
							30.4	24.3	9	1.4	3023				
139	EGR J1920+4625	290.17	46.42	77.97	14.61	0.73	16.4	4.7	55	4.2	p1	77.98	14.60	16.7	
							5.2	2.3	52	2.5	p12				

140	EGR J1921-2014	290.41	-20.24	17.79	-15.51	0.56	3.3	1.9	45	1.8	p1234				
							3.1	1.9	42	1.7	p19				
							20.3	5.9	48	4.2	20				
							30.5	8.2	55	4.6	50	17.83	-15.51	34.7	3EGJ1921-2015
141	EGR J1932-3946	293.07	-39.77	-0.91	-24.39	0.45	12.1	3.1	99	4.5	p12	-1.38	-25.12	12.4	3EGJ1935-4022
							16.2	4.5	74	4.2	p1				
							7.6	4.0	27	2.1	p2				
							11.4	8.4	9	1.6	p4				
							4.2	4.1	13	1.1	p34				
							9.2	2.5	103	4.2	p1234				
							9.2	2.5	103	4.2	p19				
							22.2	7.0	46	3.8	50				
142	EGR J1936-1515	294.24	-15.26	24.07	-16.82	0.92	57.9	19.2	26	4.0	430	24.09	-16.76	64.1	3EGJ1937-1529
							7.2	3.4	51	2.3	p1				
							3.8	2.9	34	1.4	p12				
							18.3	9.8	20	2.1	50				
143	EGR J1940-0123	295.08	-1.39	37.32	-11.50	0.73	38.4	10.5	59	4.5	330+	37.32	-11.80	42.9	3EGJ1940-0121
							24.8	7.4	65	3.8	p3				
							24.3	7.0	71	4.0	p34				
							4.3	3.0	44	1.5	p1234				
144	EGR J1949-3439	297.41	-34.66	5.58	-26.31	0.57	49.5	12.5	46	5.4	420	4.97	-26.29	51.4	3EGJ1949-3456
							16.6	4.5	77	4.4	p1				
							11.6	3.3	86	4.0	p12				
							6.8	2.6	73	2.9	p1234				
							6.8	2.6	73	2.9	p19				
							11.4	8.1	18	1.5	50				
145	EGR J1955-1338	298.78	-13.64	27.53	-20.17	0.76	22.9	6.4	57	4.3	p34	27.46	-19.54	20.2	3EGJ1955-1414
							23.2	7.0	52	4.0	p3				
							16.8	15.6	5	1.3	p4				
							7.2	2.8	68	2.8	p1234				
							7.1	2.8	67	2.8	p19				
							22.3	8.5	33	3.1	330+				
146	EGR J1959+4322	299.78	43.38	78.44	7.18	0.22	18.8	3.9	206	5.3	p12	78.33	7.14	18.5	
							11.4	6.3	44	1.9	p1				
							22.5	5.0	160	5.0	p2				
							7.6	6.1	32	1.3	p3				
							8.1	6.1	34	1.4	p34				
							15.9	3.3	240	5.2	p1234				
							15.7	3.3	238	5.2	p19				
							20.2	19.1	10	1.2	3315				
147	EGR J1959+6322	299.90	63.37	96.32	16.90	0.37	14.6	3.2	114	5.3	p19	96.51	17.00	15.1	3EGJ1959+6342
							14.6	6.8	27	2.5	p1				
							13.4	4.6	51	3.4	p2				
							18.0	9.0	21	2.3	p3				
							13.1	9.4	11	1.6	p4				
							13.6	3.8	77	4.2	p12				
							16.5	6.6	33	2.9	p34				
							14.1	3.3	108	5.1	p1234				
							32.7	28.7	5	1.5	p789				
							20.5	9.9	18	2.5	20				
148	EGR J2010-2424	302.60	-24.41	18.06	-27.53	0.76	16.8	4.4	75	4.5	p1	19.27	-26.18	16.7	3EGJ2006-2321
							7.3	5.2	15	1.5	p3				
							11.4	3.3	77	3.9	p12				
							8.3	5.3	18	1.7	p34				
							10.0	2.8	89	4.0	p1234				
							10.0	2.8	89	4.0	p19				
149	EGR J2019+3722	304.79	37.37	75.43	0.72	0.18	77.6	6.1	1282	14.2	p19	75.45	0.86	81.9	3EGJ2021+3716
							70.2	11.3	322	6.8	p1				
							71.2	9.5	490	8.3	p2				
							85.1	11.4	393	8.4	p3				
							72.0	7.3	826	10.9	p12				
							85.7	11.3	396	8.5	p34				
							75.9	6.1	1221	13.7	p1234				
							147.4	41.4	62	4.2	p56				
							57.5	13.8	180	4.5	20				
							120.9	15.7	329	8.9	328+				
							177.6	34.6	109	6.2	3315				
150	EGR J2020+4019	305.19	40.32	78.04	2.13	0.13	117.0	6.7	1867	20.0	p1234	78.03	2.16	115.0	3EGJ2020+4017
							113.3	12.7	488	10.2	p1				
							117.2	10.1	850	13.2	p2				
							117.5	12.7	516	10.6	p3				
							115.8	7.9	1339	16.7	p12				
							120.4	12.7	529	10.9	p34				
							73.2	53.1	20	1.5	p56				
							116.3	6.6	1888	20.0	p19				
							128.5	15.7	386	9.4	20				

151	EGR J2025-0810	306.25	-8.17	36.25	-24.49	0.24	132.9 72.3 22.8 21.7 21.7 11.1 22.9	17.8 35.2 3.8 3.8 3.8 6.0 13.5	323 39 141 134 135 17 14	8.6 2.2 7.5 7.0 7.0 2.2 2.0	328+ 3315 p12 p1234 p19 200 430	36.13	-24.37	26.5	3EGJ2025-0744
152	EGR J2027-4206	306.79	-42.11	-1.20	-35.00	1.12	16.3 5.2 5.4 5.2	4.8 3.0 2.8 2.8	46 26 33 32	4.2 1.9 2.1 2.1	p2 p12 p1234 p19	-1.34	-34.97	17.2	
153	EGR J2032+1226	308.02	12.44	56.25	-15.74	0.68	13.5 5.8 50.7 15.4 33.5 10.5 17.5 12.6 42.8 11.2 19.1 47.7	3.0 3.6 22.1 6.5 14.2 3.6 5.7 3.0 20.6 6.0 7.3 19.3	130 31 61 34 20 68 49 117 15 20 35 20	5.1 1.7 2.6 2.7 3.1 3.3 3.6 4.7 2.7 2.2 3.0 3.1	p19 p1 p2 p3 p4 p12 p34 p1234 p56 200 328+ 3315	56.29	-16.95	14.9	3EGJ2036+1132
154	EGR J2033+4117	308.37	41.30	80.24	0.75	0.22	51.9 49.2 49.9 55.6 49.6 56.9 44.4 51.5 48.1 79.7 60.3	6.6 12.0 10.1 12.6 7.7 12.5 43.2 6.5 15.7 18.2 38.2	828 228 357 232 584 238 18 842 135 182 31	8.4 4.4 5.3 4.8 6.8 4.9 1.1 8.4 3.3 4.8 1.7	p1234 p1 p2 p3 p12 p34 p56 p19 20 328+ 3315	80.26	0.81	52.1	3EGJ2033+4118
155	EGR J2045+0935	311.45	9.59	55.70	-20.12	0.33	11.5 12.1 16.7 15.1 9.3 17.4 11.3 21.1 11.6 14.8	2.9 3.7 7.2 9.4 3.3 5.8 2.8 11.6 7.8 9.1	98 63 29 12 56 43 100 13 15 12	4.6 3.8 2.7 1.9 3.2 3.6 4.5 2.2 1.7 1.9	p1234 p1 p3 p4 p12 p34 p19 20 328+ 4100	55.60	-20.17	10.1	3EGJ2046+0933
156	EGR J2057-4658	314.32	-46.97	-7.06	-40.56	0.28	20.4 10.3 9.1 51.7 10.4 23.4	5.8 3.4 3.2 28.1 3.2 7.1	44 46 45 10 53 38	4.4 3.5 3.3 2.7 3.8 4.2	p1 p12 p1234 p789 p19 420	-7.06	-40.56	21.3	3EGJ2055-4716
157	EGR J2200-3015	330.00	-30.25	17.73	-52.49	0.38	20.9 4.3 17.0 34.0 8.2 31.7 14.4 22.5 53.5 34.8 6.6	2.9 3.9 7.2 8.1 3.5 7.9 3.3 6.3 12.1 8.1 6.4	151 11 19 39 29 36 68 37 46 40 9	9.4 1.2 3.0 6.2 2.7 5.9 5.6 4.8 6.2 6.5 1.1	p19 p1 p2 p4 p12 p34 p1234 p56 p789 4040 420	17.72	-52.29	21.1	3EGJ2158-3023
158	EGR J2202+3340	330.63	33.68	87.10	-17.19	0.45	9.8 13.0 8.7 14.5 11.5 4.9 9.0 22.6	2.6 5.1 5.1 6.2 3.6 3.6 2.6 12.5	95 35 23 28 62 19 83 13	4.4 3.0 1.9 2.7 3.7 1.5 3.9 2.2	p19 p1 p2 p3 p12 p34 p1234 p56	87.00	-17.27	9.8	
159	EGR J2204+4225	331.01	42.43	92.88	-10.47	0.40	159.6 9.1 13.2 23.5 11.5 13.4 12.6 22.3	22.2 5.6 5.2 8.4 3.8 5.2 3.1 3.3	97 27 46 33 75 41 121 227	11.0 1.7 2.8 3.4 3.3 2.9 4.6 8.1	p56 p1 p2 p4 p12 p34 p1234 p19	92.75	-10.25	160.8	3EGJ2202+4217

160	EGR J2208+2351	332.03	23.85	81.41	-25.57	0.31	34.7	10.2	35	4.4	4100					
							12.5	3.6	59	4.2	p12					
							14.0	4.2	49	4.1	p1					
							5.7	3.7	15	1.8	p4					
							3.0	2.9	12	1.1	p34					
							7.9	2.3	70	3.9	p1234					
							13.6	8.1	13	2.0	p56					
							8.2	2.2	80	4.2	p19					
							24.8	21.2	4	1.6	260					
							5.8	3.7	15	1.8	4100					
161	EGR J2227+6114	336.76	61.24	106.44	3.08	0.30	30.4	5.3	291	6.3	p19	106.58	3.22	37.7	3EGJ2227+6122	
							30.9	10.6	70	3.2	p1					
							29.2	9.0	102	3.5	p2					
							48.0	19.7	37	2.8	p3					
							26.1	12.7	40	2.2	p4					
							30.1	6.9	173	4.8	p12					
							31.3	10.7	72	3.2	p34					
							30.1	5.8	242	5.7	p1234					
							19.5	9.7	30	2.4	p56					
162	EGR J2233-4812	338.46	-48.21	-14.70	-56.03	0.76	10.7	3.3	47	4.0	p19	-15.63	-55.71	10.8		
							23.4	9.0	21	3.5	p2					
							11.8	6.7	12	2.2	p4					
							7.6	3.6	23	2.5	p12					
							11.6	6.7	12	2.1	p34					
							8.6	3.2	35	3.2	p1234					
							29.5	17.4	9	2.3	p789					
							13.4	6.8	14	2.4	4040					
163	EGR J2234+1127	338.61	11.46	77.65	-39.08	0.17	21.7	2.8	204	9.7	p1234	77.66	-39.09	20.5	3EGJ2232+1147	
							30.8	4.6	133	8.9	p1					
							19.0	5.6	48	4.1	p3					
							9.7	4.3	25	2.7	p4					
							30.6	4.6	132	8.9	p12					
							13.9	3.5	71	4.8	p34					
							7.5	5.7	14	1.5	p56					
							18.9	2.5	212	9.3	p19					
							49.6	22.7	11	3.0	260					
							23.5	8.9	30	3.2	3200					
							9.7	4.3	25	2.7	4100					
164	EGR J2240-6734	340.13	-67.58	-40.11	-45.00	0.78	12.6	3.9	44	4.0	p12	-40.24	-44.55	13.4	3EGJ2241-6736	
							15.8	5.4	31	3.7	p1					
							7.9	5.5	12	1.6	p2					
							12.4	3.8	43	3.9	p1234					
165	EGR J2243+1519	340.96	15.33	82.99	-37.45	0.70	75.8	25.7	21	4.1	260	83.05	-37.42	76.9	3EGJ2243+1509	
							9.2	4.8	35	2.1	p1					
							7.7	5.5	19	1.5	p3					
							9.2	4.8	35	2.1	p12					
							4.1	2.7	37	1.6	p1234					
							2.9	2.4	30	1.2	p19					
							13.5	13.1	5	1.3	3360					
166	EGR J2251-1344	342.77	-13.74	52.37	-58.91	0.68	44.4	9.5	46	6.9	4040	52.81	-58.73	45.3	3EGJ2251-1341	
							4.9	4.8	6	1.2	p3					
							38.5	8.9	40	6.3	p4					
							20.1	5.0	46	5.4	p34					
							8.6	2.5	51	4.0	p1234					
							8.5	2.5	51	4.0	p19					
							13.2	9.0	7	1.8	3200					
							25.1	21.5	4	1.8	3360					
167	EGR J2253+1606	343.48	16.10	86.06	-38.22	0.19	55.5	4.0	486	18.7	p1234	86.04	-38.21	56.7	3EGJ2254+1601	
							76.4	6.8	286	15.6	p1					
							29.7	6.7	74	5.4	p3					
							50.4	6.7	127	10.8	p4					
							76.1	6.8	284	15.6	p12					
							41.3	4.8	207	11.4	p34					
							8.4	6.1	12	1.6	p56					
							48.6	3.6	492	18.1	p19					
							86.7	24.0	30	4.9	260					
							25.2	9.6	31	3.1	3200					
							20.9	15.7	8	1.6	3360					
							50.5	6.8	127	10.8	4100					
168	EGR J2256-5022	344.20	-50.38	-21.68	-58.13	1.06	22.1	7.1	25	4.4	4040	-22.26	-58.11	19.8	3EGJ2255-5012	
							17.7	6.0	25	4.1	p4					
							17.5	5.9	25	4.0	p34					
							4.9	2.4	27	2.3	p1234					
							5.2	2.4	30	2.4	p19					
							6.9	6.8	6	1.1	420					
169	EGR J2258-2745	344.54	-27.75	24.91	-64.91	0.37	157.6	26.5	60	9.8	p789	24.91	-64.91	154.8		
							9.5	4.3	21	2.6	p4					

170	EGR J2308+3645	347.23	36.76	101.03	-21.71	0.96	8.9	4.3	20	2.5	p34	4100	101.04	-21.72	22.7
							4.2	2.5	23	1.9	p1234				
							14.2	2.8	93	6.4	p19				
							8.3	4.4	15	2.2	4040				
							10.5	8.9	6	1.4	420				
							22.6	7.5	28	4.1	4100				
							22.3	7.7	28	3.8	p4				
							13.2	5.6	22	2.9	p34				
							5.9	3.0	27	2.2	p1234				
							45.8	44.5	9	1.3	p56				
171	EGR J2314+4430	348.70	44.51	105.34	-15.04	0.46	5.5	2.9	27	2.1	p19	105.31	-14.94	35.3	3EGJ2314+4426
							20.5	15.1	7	1.7	260				
							38.2	9.3	49	5.5	p4				
							28.9	7.8	47	4.7	p34				
							9.0	3.7	46	2.7	p1234				
							9.1	3.7	49	2.8	p19				
							24.8	11.2	17	2.9	4100				
172	EGR J2320-0412	350.02	-4.20	75.37	-58.36	0.58	33.8	10.1	33	4.4	3200	75.54	-58.23	34.7	3EGJ2321-0328
							13.7	4.9	31	3.5	p3				
							9.2	3.5	32	3.1	p34				
							3.4	2.2	23	1.7	p1234				
							3.6	2.2	24	1.8	p19				
							17.2	12.7	5	1.7	3360				
173	EGR J2353+3806	358.26	38.11	110.46	-23.34	0.87	37.9	10.2	40	4.9	2110	110.47	-23.34	43.0	3EGJ2352+3752
							36.6	10.0	38	4.8	p2				
							7.7	3.6	28	2.4	p12				
							5.2	3.0	25	1.9	p1234				
							4.9	2.9	23	1.8	p19				
174	EGR J2357+4602	359.38	46.04	113.25	-15.82	0.39	14.1	3.6	68	4.8	p1234	112.93	-15.54	12.8	3EGJ2358+4604
							11.7	5.0	28	2.8	p1				
							15.0	6.0	26	3.0	p2				
							21.2	10.0	14	2.8	p4				
							12.8	3.8	53	4.0	p12				
							19.1	9.8	12	2.5	p34				
							13.5	3.5	65	4.7	p19				

Table B.1. The EGR confused sources catalogue

Num 1	Name EGRc J0225+6240	RA 36.38	Dec 62.68	l 133.49	b 1.75	θ_{95} 0.34	F 30.2 42.3 24.9 23.9 38.1 35.1 29.0 32.4 21.5 25.4	σ_F 5.0 11.5 10.6 10.2 14.4 7.8 8.3 5.7 10.6 10.6	Cnts 344 100 64 63 55 173 119 292 51 65	\sqrt{TS} 6.5 4.1 2.5 2.5 2.9 4.9 3.8 6.2 2.2 2.6	vp p19 p1 p2 p3 p4 p12 p34 p1234 p56 2110	l_{sys} 133.05	b_{sys} 1.64	F_{sys} 22.1	3EG 3EGJ0229+6151
2	EGRc J0818-4613	124.74	-46.23	-97.25	-5.73	0.31	29.8 27.8 44.6 37.5 22.5 44.3 27.9 47.1	5.7 7.3 10.8 25.4 6.9 10.0 5.7 13.1	368 199 168 24 179 194 348 122	5.6 4.0 4.5 1.6 3.4 4.8 5.2 3.9	p1234 p1 p3 p4 p12 p34 p19 3385	-97.25	-5.73	25.8	
3	EGRc J0842-4501	130.66	-45.03	-95.78	-1.68	0.26	113.9 98.7 148.7 123.8 192.6 104.9 131.9 114.1 120.4	10.1 13.7 36.5 17.3 52.9 12.8 16.5 10.1 21.0	1360 630 135 492 97 765 590 1343 328	12.2 7.7 4.5 7.7 4.0 8.7 8.6 12.1 6.2	p19 p1 p2 p3 p4 p12 p34 p1234 3385	-95.18	-1.47	67.5	
4	EGRc J0912+7146	138.15	71.77	141.44	36.44	0.62	7.1 8.2 2.4 12.4 12.7 4.9 12.9 6.7 8.0 12.2	1.6 2.8 2.2 4.5 8.4 1.8 4.0 1.6 5.2 4.5	130 53 16 35 9 64 45 111 15 34	5.1 3.3 1.2 3.3 1.9 3.1 3.9 4.7 1.8 3.2	p19 p1 p2 p3 p4 p12 p34 p1234 p56 319+	141.85	36.29	5.5	
5	EGRc J0927+6054	141.91	60.91	153.55	42.15	0.67	5.1 4.1 3.9 9.0 16.2 4.0 10.6 5.2 2.7	1.5 2.4 2.1 4.8 8.3 1.5 4.1 1.5 2.2	81 24 30 16 12 54 27 86 17	4.0 1.9 2.1 2.2 2.6 2.9 3.2 4.0 1.3	p1234 p1 p2 p3 p4 p12 p34 p19 227+	153.38	42.50	4.4	
6	EGRc J1038-5724	159.61	-57.41	-74.25	0.96	0.40	33.1 23.9 34.5 35.0 27.1 25.5 33.3 28.3 43.8 120.5	5.4 8.2 17.3 11.3 19.9 7.4 9.8 5.9 12.9 54.4	455 129 44 114 25 171 139 307 117 24	6.6 3.1 2.1 3.3 1.5 3.6 3.6 5.1 3.7 2.7	p19 p1 p2 p3 p4 p12 p34 p1234 p56 p789	-74.25	0.96	38.6	
7	EGRc J1233-0318	188.46	-3.30	-65.69	59.28	1.04	10.4 7.3 4.6 3.2 4.3	2.9 2.3 1.5 1.3 3.7	78 79 97 90 17	4.1 3.6 3.4 2.6 1.3	p1 p12 p1234 p19 virgo3a	-64.78	58.36	9.8	3EGJ1230-0247
8	EGRc J1255-0404	193.78	-4.08	-55.30	58.78	0.71	9.3 11.6 7.9 8.0 3.6 6.4 15.2	1.9 4.7 3.3 3.3 2.4 2.0 4.6	272 83 43 88 36 134 103	5.3 2.6 2.7 2.6 1.6 3.3 3.6	p19 p1 p4 p12 p34 p1234	-55.24	58.82	8.9	
9	EGRc J1332-1217	203.04	-12.29	-41.69	49.36	0.56	5.9 6.9 4.5 3.6 14.7	1.6 3.3 2.2 2.4 1.7	112 33 40 54 52	4.0 2.3 2.2 2.3 3.5	p19 p1 p12 p1234 p56	-41.67	49.37	7.5	
10	EGRc J1740-2851	265.05	-28.85	-0.55	1.05	0.16	70.6 52.7	6.3 10.8	1750 402	11.8 5.1	p19 p1	-0.27	1.13	45.7	3EGJ1736-2908

11	EGRc J1747-2852	266.76	-28.88	0.21	-0.24	0.23	69.5 90.0 70.6 59.7 83.3 69.9 84.9 42.1 102.8 50.5 62.8 72.4 140.7 66.9 111.5	13.9 12.6 17.0 8.6 10.1 6.5 24.0 14.4 23.6 29.8 49.4 26.6 31.0 38.1 47.6	350 615 234 757 846 1595 168 169 210 51 28 97 156 42 51	5.3 7.7 4.4 7.4 8.8 11.3 3.8 3.1 4.7 1.8 1.4 2.9 5.1 1.9 2.5	p2 p3 p4 p12 p34 p1234 p56 50 330+ 4230 2230 2260 3023 4210 4235	p19	-0.01	-0.47	146.2	3EGJ1746-2851
12	EGRc J2025+3559	306.48	35.99	75.07	-1.18	0.46	86.7 78.7 73.8 81.8 132.0 76.6 95.8 84.8 124.3 67.8 130.9 91.1 155.0 62.1 56.2 209.4 140.5 149.1	6.0 10.4 13.3 11.4 17.1 8.2 9.5 6.2 23.8 13.5 21.5 29.5 49.1 25.5 35.1 66.0 39.3 50.7	2158 601 360 586 432 958 1000 1947 240 282 294 92 70 79 40 49 88 59	15.7 8.2 6.0 7.7 8.7 10.1 11.0 14.8 5.7 5.4 6.7 3.4 3.6 2.6 1.7 3.8 4.0 3.3	p19 p1 p2 p3 p4 p12 p34 p1234 p56 50 330+ 4230 2230 2260 2310 4210 4235	75.22	-1.09	40.6	3EGJ2027+3429	
13	EGRc J2215+0653	333.81	6.89	69.17	-39.16	0.59	40.8 33.9 43.5 10.5 11.5 32.0 31.6 31.3	6.6 10.1 8.7 9.7 9.7 5.5 5.4 12.6	459 155 290 47 52 504 515 95	6.6 3.6 5.4 1.1 1.2 6.2 6.2 2.6	p12 p1 p2 p3 p34 p1234 p19 20	69.01	-38.58	18.2		
14	EGRc J2249+1724	342.39	17.41	85.89	-36.55	0.42	18.5 10.9 3.8 3.0 18.6 26.2 10.2 9.8 14.5 13.7 12.9 31.0	5.7 3.7 2.1 1.9 5.7 6.7 5.4 5.4 4.2 3.4 3.0 9.8	36 44 32 30 36 63 36 35 73 118 128 37	4.1 3.5 2.0 1.8 4.1 4.8 2.0 2.0 3.9 4.5 4.7 4.0	p4 p34 p1234 p19 4100 p3 p1 p12 p34 p1234 p19 3200	85.93	-36.41	24.8	3EGJ2248+1745	